Research Square

Preprints are preliminary reports that have not undergone peer review.
They should not be considered conclusive, used to inform clinical practice,
or referenced by the media as validated information.

Comparative Performance Evaluation of Barium Strontium Titanate Thin-Film Metal–Insulator–Metal Capacitors with Different Dielectric Thicknesses and a Fixed-Thickness Interdigital Capacitor

Abdullah .

p22ee001@iitj.ac.in

Indian Institute of Technology Jodhpur https://orcid.org/0000-0001-9487-2595

Research Article

Keywords: Barium strontium titanate, metal–insulator–metal capacitor, interdigital capacitor, RF magnetron sputtering, dielectric constant, capacitance density

Posted Date: July 21st, 2026

DOI: https://doi.org/10.21203/rs.3.rs-10395864/v1

License: This work is licensed under a Creative Commons Attribution 4.0 International License.
Read Full License

Additional Declarations: The authors declare no competing interests.

Abstract

Barium strontium titanate (BST) thin films are promising dielectric materials for radio-frequency (RF), microwave, and integrated passive devices because of their high dielectric permittivity and excellent electrical tunability. In this work, the electrical performance of BST-based metal–insulator–metal (MIM) capacitors with dielectric thicknesses of 50, 70, and 170 nm was systematically compared with that of a 100 nm BST-based interdigital capacitor (IDC) fabricated on platinized silicon substrates. BST thin films were deposited by radio-frequency magnetron sputtering, followed by the deposition of Cr/Au (40/200 nm) electrodes using thermal evaporation. The fabricated devices were characterized through capacitance–voltage, conductance–voltage, capacitance density, dielectric constant, dielectric loss, quality factor, electric field, normalized capacitance, and frequency-dependent measurements. The 50 nm BST MIM capacitor exhibited the highest capacitance density (≈ 0.074 F m^{-2}), the highest quality factor (≈ 3.1 at 1 MHz), and a maximum electric field of ≈ 6 MV cm^{-1}, whereas the 170 nm BST capacitor achieved the highest dielectric constant (≈ 1090 at 500 kHz). The dielectric loss of all the manufactured devices decreased dramatically with an increase in frequency, showing high-frequency behavior. Interdigital BST capacitor with a thickness of 100 nm showed stable capacitance and conductance with insignificant bias dependence in the studied frequency range. The study shows that the thickness of the dielectric layer and capacitor structure have a strong impact on the electrical properties of BST thin-film capacitors. Lower dielectric thickness provides better capacitance density and quality factor, while higher thickness increases the dielectric permittivity.

1. Introduction

The fast evolution of wireless communication technology in the form of fifth-generation (5G), sixth-generation (6G) technology, radars, satellites, IoT, etc., has led to a growing need for miniaturized, low-loss, and highly tuneable passive RF-microwave components. In such components, capacitors find application in filter circuits, phase-shifters, impedance matching circuitry, voltage-controlled oscillators, resonators, and storage circuits. As a result, the search for dielectric materials with high permittivity, low dielectric loss, high breakdown strength, and high frequency stability is an ongoing research area **[1]–[4]**.

Barium Strontium Titanate (BST), which is written chemically as $Ba_{1-x}Sr_xTiO_3$, has been found to be one of the most potential ferroelectric lead-free materials due to its high dielectric constant, low leakage current, dielectric tuning ability, and suitability for silicon-based microelectronics **[5], [6]**. The Ba/Sr ratio controls the dielectric property of BST within a wide range of frequency and temperatures, which makes it a suitable material for RF/microwave integrated circuits. Moreover, BST thin films can be fabricated by various techniques like radio-frequency magnetron sputtering, pulsed laser deposition, chemical solution deposition, and molecular beam epitaxy **[5], [7].**

Metal-Insulator-Metal (MIM) capacitors have been extensively studied due to their simple device structure, high capacitance density, low parasitic resistance, and compatibility with CMOS fabrication technology. The electrical characteristics of MIM capacitors rely highly on the dielectric material,

dielectric thickness, electrode material, interface properties, and fabrication processes. In BST MIM capacitors, a decrease in dielectric thickness leads to an increase in the capacitance density, while increased dielectric thickness improves the breakdown voltage and decreases leakage current. Hence, dielectric thickness is one of the critical parameters for achieving the optimum balance between capacitance density and dielectric loss **[8], [9]**.

A number of recent investigations have centered on enhancement of BST dielectric properties using material engineering techniques. Ta donor doping is claimed to increase the dielectric constant almost two times along with improvement in capacitance density and breakdown field in deposited $BaTiO_3$ MIM thin-film capacitors, thus showing that defect engineering can effectively be used for development of high performance dielectric materials **[10]**. In a similar manner, phase boundary engineering in BST thin films grown epitaxially resulted in dielectric tunability of up to 91% along with breakdown fields close to 800 kV/cm at the same time **[6]**.

In addition to compositional engineering, another important aspect that significantly affects the electrical properties of BST capacitors is the choice of electrodes. Comparing different electrodes, such as Ag, Cu, In, and $MoSi_2$, it was found that electrodes based on Ag provide the best capacitance density and dielectric constant, while those made from In provide the lowest dielectric loss due to better interface properties between metals and BST dielectric layer **[11]**. Moreover, the properties of amorphous BST thin films were thoroughly studied using impedance spectroscopy; it was established that the dielectric response of BST materials is affected by oxygen vacancies, defect complexes, and interfaces with electrodes **[12]**.

In addition to traditional parallel-plate MIM capacitors, another type of capacitor, i.e., interdigital capacitors (IDCs), have gained much interest due to their planar design, simple fabrication, large sensing area, and applicability for RF integrated circuitry. In contrast to MIM capacitors, the electric field in IDCs is predominantly oriented laterally by means of fringing fields, and thus the capacitance of such a structure depends greatly on the shape of the electrodes and their surface dielectrics. All these features make IDC structures highly attractive for application in microwave resonators, tunable filters, and sensors **[2], [3]**. Nevertheless, few comparative studies of conventional BST thin-film MIM capacitors and BST-IDCs are known to exist.

Even though there have been many successful results in enhancing BST dielectric properties via compositional, electrode, and defect engineering, there have not been many studies done regarding the effects of the dielectric thickness on the electrical properties of BST thin film MIM capacitors or comparison of BST thin film MIM capacitors with interdigital capacitor structures of the same thickness. It is crucial to perform a comparative study in order to choose the best capacitor structure for RF, microwave, and integrated passive devices.

In the current study, BST films having dielectric layers of 50 nm, 70 nm, and 170 nm thickness were grown onto platinized silicon substrates using radio-frequency magnetron sputtering technique for preparing circular Metal–Insulator–Metal capacitors using Cr/Au (40/200 nm) electrodes. At the same

time, an interdigital capacitor was prepared using BST film having 100 nm thickness on the same substrate using same electrode materials through shadow mask method. These devices have been thoroughly investigated using capacitance-voltage, conductance-voltage, capacitance density, dielectric constant, dielectric loss, quality factor, electric field, and normalized capacitance measurement techniques at different operating frequencies. Comparison study carried out in this work is very useful for understanding the impact of dielectric thickness and device structure on BST capacitor behavior in future RF/microwave electronics.

2. Experimental Procedure

2.1 Materials and Thin-Film Deposition

The BST thin films were grown on commercially available platinized silicon (Pt/Si) substrates by radio frequency (RF) magnetron sputtering technique. The Pt/Si substrates were initially diced into appropriate sizes before the deposition process. The substrate wafers were then cleaned by following the regular ultrasonic cleaning protocol. Initially, the substrates were subjected to ultrasonic cleaning in acetone followed by IPA to remove any remaining organic contaminants. Then, the substrates were further rinsed using DI water and finally dried using high purity N_2 gas.

The commercial BST ceramic target of size 2 inches was used for sputtering process. The cleaned substrates were mounted on the rotating holder kept above the target to ensure that the thin films are deposited uniformly throughout the substrate surface. The BST thin films of 50 nm, 70 nm, and 170 nm thickness were prepared under room temperature with Ar gas. The sputtering process was carried out at an RF power of 100 W, with an argon gas flow rate of 60 SCCM. Prior to deposition, the sputtering chamber was evacuated to a base pressure of 2×10^{-6} mbar, while the deposition was performed at a working pressure of 2.0×10^{-2} mbar. Continuous substrate rotation during deposition ensured improved thickness uniformity and minimized film non-uniformity across the substrate surface.

Following BST deposition, circular top electrodes were fabricated using a thermal evaporation system. A chromium/gold (Cr/Au) metal stack with thicknesses of 40 nm/200 nm was deposited through a precision shadow mask to define circular metal–insulator–metal (MIM) capacitor structures with a diameter of 500 μm. Chromium was used as the adhesion layer, whereas gold served as the top conducting electrode because of its excellent electrical conductivity and chemical stability. The thermal evaporation process was performed at a chamber pressure of 2.3×10^{-6} mbar, ensuring high-purity metal deposition and good metal–dielectric interface quality.

The complete fabrication process resulted in BST thin-film metal–insulator–metal capacitors with three different dielectric thicknesses (50 nm, 70 nm, and 170 nm), which were subsequently used for detailed electrical characterization.

2.2 Device Fabrication

(a) Metal–Insulator–Metal (MIM) Capacitor Fabrication

After the deposition of the BST dielectrics, metal-insulator-metal (MIM) capacitor structures were then fabricated on the platinized silicon substrates. Platinized silicon substrate is used as the bottom electrode, while the deposited BST thin film is the dielectric. Three sets of MIM capacitors have been fabricated employing BST dielectric thickness of 50 nm, 70 nm, and 170 nm, so as to study the effect of dielectric thickness on the electrical properties of these devices. Circular top electrodes were then deposited using thermal evaporation with the aid of a precise shadow mask, utilizing chromium/gold (Cr/Au) metal stack of thickness 40 nm/200 nm respectively. Chromium was used as the adhesion layer between the BST dielectric and the gold electrode, while gold is the highly conductive top electrode. The deposited circular top electrodes have a diameter of 500 μm, hence the active capacitor area. Hence the final device structure was made up of Cr/Au/BST/Pt/Si metal insulator metal, giving a parallel plate capacitor.

(b) Interdigital Capacitor (IDC) Fabrication

As a comparator to the traditional MIM capacitor, a planar interdigital capacitor (IDC) was also fabricated on a platinized silicon substrate. To begin with, a 100 nm BST thin film was first deposited on the substrate using the same RF magnetron sputtering technique discussed in Section 2.1. After the deposition of the BST thin film, a metal Cr/Au (40 nm/200 nm) was deposited in a shadow mask pattern through thermal evaporation process. As such, the fabricated IDC is made up of parallel interdigital fingers having an equal inter-finger separation of 100 μm, thus allowing the creation of lateral fringing electric fields in the BST dielectric film. As opposed to the parallel plate electric field structure of the MIM capacitor, the capacitance of the IDC is dominated by the fringing electric fields between neighbouring electrodes. The completed IDC structure can therefore be represented as a Cr/Au/BST/Pt/Si planar capacitor, allowing a direct comparison between the electrical performance of conventional MIM capacitors and fixed-thickness interdigital capacitors fabricated under identical material and processing conditions.

The fabrication process flow diagrams as well as the corresponding cross-sections of the fabricated MIM and interdigital capacitors are shown in Fig. 1 and Fig. 2, respectively. With regard to identical deposition of BST and same electrode material used in both capacitors, the variations in electrical properties observed should be attributed to variations in the dielectric thickness and geometry of the capacitor.

2.3 Electrical Characterization

The electrical properties of the fabricated BST thin film MIM capacitors and the BST thin film interdigital capacitor (IDC) were examined using the Keithley 4200A-SCS Parameter Analyzer coupled with Clarius™ V1.9.1 software. The measurements of the electrical properties were done at room temperature in order to assess the impact of the thickness of the dielectric layer and device structure on its capacitive properties.

For the MIM capacitor structures, electrical measurements were performed on BST dielectric thicknesses of 50 nm, 70 nm, and 170 nm. The capacitance–voltage (C–V) characteristics were recorded over a bias voltage range of − 20 V to + 30 V at measurement frequencies of 10 kHz, 50 kHz, 500 kHz, and 1 MHz. In addition, the capacitance–frequency (C–f) characteristics were measured to investigate the frequency-dependent dielectric response of the fabricated capacitors. From the measured capacitance data, the conductance (G), capacitance density (C/A), dielectric constant (ε_r), dielectric loss (tan δ), quality factor (Q), electric field (E), and normalized capacitance (C/C_o) were calculated to comprehensively evaluate the electrical performance of the BST thin-film capacitors.

The electrical characterization of the BST interdigital capacitor (IDC) was performed under identical room-temperature conditions. The capacitance–voltage (C–V) and conductance–voltage (G–V) characteristics were measured over a bias voltage range of − 20 V to + 20 V at frequencies ranging from 100 kHz to 1 MHz. Furthermore, the capacitance–frequency (C–f) and conductance–frequency (G–f) characteristics were obtained at applied bias voltages of 5 V, 10 V, 15 V, 20 V, and 30 V to investigate the frequency-dependent electrical response of the interdigital capacitor.

The dielectric constant of the BST thin films was calculated from the measured capacitance using the parallel-plate capacitor relation

$$\epsilon_r = \frac{Cd}{\epsilon_0 A},$$

1

where $C$is the measured capacitance, $d$is the BST dielectric thickness, $A$is the active electrode area, and $\epsilon_0$is the permittivity of free space. The capacitance density was determined using

$$\frac{C}{A} = \frac{\epsilon_0 \epsilon_r}{d},$$

2

while the quality factor was calculated from the measured dielectric loss according to

$$Q = \frac{1}{\tan\delta}.$$

3

The measured data were processed and analyzed using OriginLab software, which was employed for data visualization, graphical representation, and comparative analysis of the electrical characteristics of the fabricated MIM and interdigital capacitor structures.

Figure 2. Schematic illustration of the BST-based interdigital capacitor (IDC) fabricated on a platinized silicon substrate. The device comprises a 100 nm BST dielectric film deposited by RF sputtering, with Cr/Au (40/200 nm) interdigital electrodes patterned on the dielectric layer by thermal evaporation through a shadow mask. The interdigital electrode geometry employs an E-shaped finger configuration with a constant inter-finger spacing of 100 μm. The figure includes the top-view electrode pattern, three-dimensional schematic, and cross-sectional view of the device architecture.

Figure 2 illustrates the schematic architecture of the fabricated BST-based interdigital capacitor (IDC) on a platinized silicon substrate. The device consists of a 100 nm BST dielectric layer with Cr/Au (40/200 nm) E-shaped interdigital electrodes separated by a uniform finger-to-finger spacing of 100 μm. The top-view, three-dimensional, and cross-sectional schematics highlight the planar device configuration employed for electrical characterization.

3. Result and Analysis

Figure 3 illustrates the capacitance–voltage (C–V) characteristics of the barium strontium titanate (BST) thin-film metal–insulator–metal (MIM) capacitors with dielectric thicknesses of 50 nm, 70 nm, and 170 nm, measured over a bias voltage range of − 20 V to + 30 V at frequencies of 10 kHz, 50 kHz, 500 kHz, and 1 MHz. All three devices exhibit a pronounced voltage-dependent capacitance with an abrupt transition occurring close to 0 V, indicating strong electric-field-induced modulation of the dielectric response. The observed behavior is characteristic of ferroelectric/paraelectric BST thin films, where the dielectric permittivity varies with the applied electric field because of polarization reorientation and domain-wall dynamics **[13], [14]**.

For the 50 nm BST dielectric **(**Fig. 3**(a))**, the capacitance decreases gradually under negative bias and exhibits a sharp drop near 0 V, followed by an almost constant value under positive bias. At 500 kHz, the capacitance changes from approximately − 3.8×10^{-9} F at − 20 V to − 14.5×10^{-9} F after the transition. Similarly, the capacitance at 10 kHz changes from approximately − 2.6×10^{-9} F to − 11.8×10^{-9} F, while the values measured at 50 kHz and 1 MHz stabilize near − 6.2×10^{-9} F and − 4.8×10^{-9} F, respectively. The larger capacitance variation observed for the thinner dielectric indicates a stronger electric-field interaction across the BST layer, which enhances polarization switching and dielectric tunability.

The 70 nm BST capacitor **(**Fig. 3**(b))** exhibits a similar voltage dependence; however, the overall capacitance variation is smaller than that of the 50 nm film. Following the transition near zero bias, the capacitance stabilizes at approximately − 4.2×10^{-9} F (500 kHz), − 3.2×10^{-9} F (1 MHz), − 2.6×10^{-9} F (10 kHz), and − 1.3×10^{-9} F (50 kHz). With regard to the effect on the capacitance, the decrease in capacitance can be said to be due to the increase in thickness of the dielectric because capacitance is inversely proportional to the dielectric thickness ($C = \varepsilon_0 \varepsilon_r A/d$). The increase in thickness of the BST thus results in a lower electric field for the dielectric for the same applied voltage, hence lower capacitance.

For the 170 nm BST film (Fig. 3**(c))**, the lowest capacitance values are observed among the three devices. The capacitance measured at 500 kHz decreases from approximately − 3.0 × 10^{-9} F under negative bias to approximately − 11.2 × 10^{-9} F after the voltage transition, whereas the capacitance measured at 10 kHz, 1 MHz, and 50 kHz stabilizes near − 8.1 × 10^{-9} F, − 4.6 × 10^{-9} F, and − 0.8 × 10^{-9} F, respectively. The thicker dielectric layer suppresses the electric-field intensity across the BST film, resulting in reduced polarization response and lower capacitance variation. In addition, the relatively smooth capacitance response at higher frequencies suggests that interfacial polarization and slow dipolar relaxation mechanisms contribute less significantly under rapidly alternating electric fields **[12], [16]**.

The frequency dependence observed in all three devices further confirms that capacitance decreases with increasing frequency because the dipolar and space-charge polarization mechanisms cannot follow the rapidly varying electric field. With regard to low frequency operation, the above mentioned polarization mechanisms play a significant role in the dielectric behavior of the structure and result in higher capacitance value, while in the case of high frequency operation the electronic and ionic polarization mechanisms dominate **[3],[12]**. Also, the abrupt transition taking place around zero bias voltage irrespective of the dielectric thickness demonstrates electric-field-assisted polarization switching in BST dielectric, in line with the observations reported earlier by other researchers for BST thin film MIM capacitors and microwave tunable dielectrics **[6],[13]**. Thus, it can be concluded that dielectric thickness plays a key role in determining the voltage dependence of the capacitance of the BST dielectric material, where the smaller dielectric thickness leads to higher capacitance value due to the higher electric field across the dielectric layer.

Figure 4 presents the conductance–voltage (G–V) characteristics of the barium strontium titanate (BST) thin-film metal–insulator–metal (MIM) capacitors with dielectric thicknesses of 50 nm, 70 nm, and 170 nm, measured over a bias voltage range of − 20 V to + 30 V at frequencies of 10 kHz, 50 kHz, 500 kHz, and 1 MHz. In all three devices, the conductance increases gradually as the applied voltage approaches 0 V from the negative bias region, followed by a sharp transition near zero bias and a nearly constant conductance in the positive bias region. This behavior indicates field-dependent charge transport across the BST dielectric layer and suggests a transition from a low-conductance state under reverse bias to a higher-conductance state under forward bias.

For the 50 nm BST film (Fig. 4**(a))**, the highest conductance is observed at 50 kHz, reaching approximately 0.062 S after the transition, followed by 500 kHz (~ 0.041 S), 10 kHz (~ 0.040 S), and 1 MHz (~ 0.010 S). The gradual increase in conductance under negative bias indicates enhanced carrier transport with increasing electric field, whereas the abrupt increase near 0 V may be attributed to the alignment of polarization domains and increased availability of charge carriers at the metal–dielectric interface. The significantly lower conductance at 1 MHz suggests that space-charge and dipolar polarization mechanisms are unable to follow the rapidly alternating electric field, thereby reducing the AC conduction.

As far as the 70 nm BST film (Fig. 4**(b))** is concerned, the total conductance shows a decrease when compared to the 50 nm sample. Following the voltage switching, the conductance remains steady at around 0.032 S (500 kHz), 0.031 S (10 and 50 kHz), and 0.018 S (1 MHz). This decrease in the conductance with an increase in the thickness of the dielectric layer is logical as the increased thickness of the BST film leads to increased electrical resistance and decreased electric field through the dielectric.

The 170 nm BST capacitor (Fig. 4**(c))**, on the other hand, shows lower conductance values compared to the other two thicknesses except for a particular fluctuation experienced after the voltage transition at 50 kHz. At 10 kHz, 500 kHz, and 1 MHz, the conductance value is around 0.051 S, 0.041 S, and 0.012 S, respectively. This unusual conductance fluctuation could be attributed to the dielectric relaxation, localized trapping/de-trapping of charges, or interface states in the thick BST dielectric layer.

In general, the conductivity falls with the increase in test frequency, especially at 1 MHz where all the samples show the minimum values. The reasons behind such a decrease include the decreased effect of interfacial and space-charge polarizations at high frequencies since they cannot respond quickly enough to the oscillating field. Also, the increase of the thickness of the BST dielectric film from 50 nm to 170 nm decreases the conductivity due to the increased transport distance and the decreased leakage current across the dielectric film. In conclusion, dielectric thickness is a critical factor that determines the conduction properties of BST MIM capacitors.

Figure 5 presents the capacitance density–voltage (C/A–V) characteristics of the BST thin-film metal–insulator–metal (MIM) capacitors with dielectric thicknesses of 50 nm, 70 nm, and 170 nm, measured over a bias voltage range of − 20 V to + 30 V at frequencies of 10 kHz, 50 kHz, 500 kHz, and 1 MHz. Similar to the capacitance–voltage characteristics, all devices exhibit a gradual increase in capacitance density under negative bias followed by a sharp transition near 0 V, after which the capacitance density becomes nearly constant. This kind of behavior proves that there exists a significant dependency of dielectric polarization on electric fields **[13], [14]**.

The maximum capacitance density of the 50 nm BST capacitor (Fig. 5**(a))** is achieved at 500 kHz frequency and equals about 0.074 F/m² after the transition of the voltage. Under the same bias, the stable capacitance density values for 10 kHz, 50 kHz, and 1 MHz frequencies equal 0.060 F/m², 0.031 F/m², and 0.025 F/m² respectively. For negative bias, the capacitance density value gradually increases from 0.020 F/m² at -20 V to 0.040 F/m² at about 0 V before the sharp increase. It should be noted that the high capacitance density of the thin film 50 nm capacitor is justified by the inverse proportionality of the capacitance density to the thickness of dielectric material $C/A = \varepsilon_0\varepsilon_r/d$ **[15]**.

In regard to the 70 nm BST capacitor (Fig. 5**(b))**, capacitance density becomes lower than in the case of the 50 nm capacitor. Post-voltage change, the values of the capacitance density become 0.021 F/m2 at 500 kHz, 0.016 F/m2 at 1 MHz, 0.013 F/m2 at 10 kHz, and 0.006 F/m2 at 50 kHz. However, the dependence on the voltage is still the same, while the increased dielectric thickness decreases the value of the electric field through the BST layer and, thus, the charge per unit of the electrode area.

For the 170 nm BST capacitor **(**Fig. 5**(c))**, capacitance density is the least compared to the other two dielectric thicknesses. This is consistent with the relation between capacitance density and dielectric thickness, which is inversely proportional. Following the voltage transition, the capacitance density remains constant at about 0.057 F/m² at 500 kHz, 0.042 F/m² at 10 kHz, 0.023 F/m² at 1 MHz, and 0.004 to 0.006 F/m² at 50 kHz. The reason for the decreased capacitance density for the thicker BST layer is due to the higher dielectric thickness, thereby reducing the electric field intensity, which, in turn, reduces the polarization charge in the dielectric layer. The slight oscillation recorded in the capacitance density at 50 kHz could be due to dielectric relaxation or charge trapping near the metal/dielectric interface, as has been reported in BST thin-film capacitors **[12, 16]**.

Comparing all three thicknesses of the dielectrics, it is possible to conclude that the capacitance density for the 50 nm BST layer is highest, which means that thin dielectrics offer higher storage capacity. Despite having lower capacitance density than the other two, the response of the 170 nm layer is relatively stable throughout the whole range of the applied voltage. In all three capacitors, the voltage-induced transition occurring near 0 V reflects electric-field-dependent polarization within the BST dielectric, while the nearly constant capacitance density at positive bias suggests saturation of polarization under higher electric fields. Overall, these results demonstrate that dielectric thickness is the dominant parameter governing capacitance density, whereas measurement frequency primarily influences the magnitude of the dielectric polarization through the frequency-dependent response of dipolar and space-charge polarization mechanisms **[3], [10], [16]**. The superior capacitance density achieved by the 50 nm BST film makes it particularly attractive for high-density integrated capacitors and RF passive components where maximum charge storage per unit area is required.

Figure 6 shows the quality factor (Q-factor) as a function of applied bias voltage for the BST thin-film metal–insulator–metal (MIM) capacitors with dielectric thicknesses of 50 nm, 70 nm, and 170 nm, measured over a voltage range of − 20 V to + 30 V at frequencies of 10 kHz, 50 kHz, 500 kHz, and 1 MHz. In contrast to the capacitance and conductance characteristics, the Q-factor remains nearly constant throughout the applied voltage range for all dielectric thicknesses, indicating that the AC energy dissipation of the fabricated capacitors is only weakly influenced by the applied DC bias. This almost voltage-insensitive nature indicates that the loss mechanisms in the dielectric are fairly constant for the entire range of voltages studied and there is no degradation or instability due to electric field induced in the BST dielectric layer **[13], [16]**.

In relation to the 50 nm BST film **(**Fig. 6**(a))**, the maximum Q-factor value is achieved for 1 MHz frequency (Q = ~ 3.10), followed by 500 kHz (~ 1.10), whereas very low Q-factors of ~ 0.03 and ~ 0.01 are found for 50 kHz and 10 kHz, respectively. The almost negligible dependence on the bias voltage suggests that the dielectric loss is practically constant across the entire bias voltage range. In the case of the 70 nm BST capacitor **(**Fig. 6**(b))**, the Q-factor values are of about ~ 1.10 for 1 MHz, ~ 0.41 for 500 kHz, and < 0.02 for both 10 kHz and 50 kHz, with the slight fluctuation near 0 V due to possible measurement uncertainty or polarization switching transients. Finally, for the 170 nm BST film **(**Fig. 6**(c))**, again a voltage-independent

Q-factor behavior is observed for values of ~ 2.35 for 1 MHz, ~ 0.87 for 500 kHz, and < 0.02 for lower frequencies.

In comparing all three dielectric thicknesses, one will observe that the Q-factor is higher in the 50nm BST capacitor, while the lowest values of the Q-factor will be found in the 70nm dielectric, especially at higher frequencies. This can be due to the low value of the equivalent series resistance and strong capacitive effect of the thinner dielectric. Since the quality factor is inversely proportional to the dielectric loss $(Q = 1/\tan\delta)$, the higher Q-factor obtained at 1 MHz indicates reduced dielectric loss and improved high-frequency performance of the fabricated BST capacitors **[10], [13]**. Moreover, the nearly constant Q-factor with increasing bias voltage confirms that the dielectric loss is primarily governed by intrinsic polarization mechanisms rather than by the applied electric field.

Overall, the Q-factor results demonstrate that frequency has a much greater influence than applied voltage on the energy-storage efficiency of the fabricated BST MIM capacitors. The stable Q-factor over the entire bias range further indicates good dielectric stability and reliable capacitor operation, while the comparatively higher Q-factor obtained for the 50 nm BST dielectric suggests that thinner BST films are more suitable for RF and microwave capacitor applications requiring low dielectric loss and efficient energy storage **[7], [10], [13]**.

Figure 7 presents the dielectric constant–voltage (ε_r–V) characteristics of the BST thin-film metal–insulator–metal (MIM) capacitors with dielectric thicknesses of 50 nm, 70 nm, and 170 nm, measured over a bias voltage range of − 20 V to + 30 V at frequencies of 10 kHz, 50 kHz, 500 kHz, and 1 MHz. The dielectric constant was calculated from the measured capacitance using the parallel-plate capacitor relation. All three capacitors exhibit a pronounced electric-field-dependent dielectric response, characterized by a gradual increase in dielectric constant under negative bias followed by a sharp rise near 0 V, after which the dielectric constant remains nearly constant throughout the positive bias region. This behavior is characteristic of BST ferroelectric thin films, where polarization alignment and electric-field-induced dielectric tunability dominate the dielectric response **[13], [14]**.

For the 50 nm BST dielectric **(**Fig. 7**(a))**, the dielectric constant exhibits the highest values at 500 kHz, increasing from approximately 110 at − 20 V to nearly 420 after the voltage transition. At 10 kHz, the dielectric constant increases from approximately 80 to 340, while values of approximately 180 and 140 are obtained at 50 kHz and 1 MHz, respectively. The rapid increase near zero bias indicates enhanced dipole alignment and polarization switching within the BST layer, resulting in a substantial increase in dielectric permittivity under an applied electric field.

BST capacitor of 70 nm **(**Fig. 7**(b))** has relatively low values for its dielectric constant. After crossing 0 V point the dielectric constant attains steady state values of about 170 at 500 kHz, 125 at 1 MHz, 105 at 10 kHz, and 50 at 50 kHz. This decrease in dielectric constant when compared with that of 50 nm film could be attributed to some changes in the structure of film, crystalline nature of film, interfaces, and decrease in strength of electric field due to increased thickness of dielectric layer **[10], [15]**.

Regarding the 170 nm BST dielectric (Fig. 7**(c))**, the value of the dielectric constant is higher compared to other two devices. After the voltage change, the value of the dielectric constant becomes about 1090 at 500 kHz, 800 at 10 kHz, 450 at 1 MHz, and changes from 50 to 120 at 50 kHz. The highest value of the dielectric constant at 500 kHz indicates that the higher thickness of the BST dielectric provides the increased value of dielectric polarization, due to the increase in crystallinity, volume of polarization, and decreased influence of depolarization. The fluctuation at 50 kHz can be caused by dielectric relaxation, interface states, or charge trapping in the dielectric layer **[12], [16]**.

It can be seen from the comparison of the three different thicknesses of dielectric films that the dielectric effect is heavily dependent on thickness and frequency. The 50 nm thick film has quite a high dielectric constant and a high value for its electric field effect, but the 170 nm thick film gives the highest dielectric constant, showing that the dielectric permittivity does not depend only on thickness but also on intrinsic properties of the material like crystallographic texture, density of defects, etc. This observation agrees with previous reports showing that optimized BST microstructures can significantly enhance dielectric polarization and tunability even in relatively thick dielectric layers **[6], [9], [13]**. Furthermore, the nearly constant dielectric constant under positive bias indicates saturation of polarization, whereas the gradual variation under negative bias reflects progressive domain alignment and electric-field-induced polarization within the BST dielectric.

Overall, the results confirm that the dielectric constant of BST thin-film MIM capacitors is strongly dependent on both applied electric field and microstructural properties. The remarkably high dielectric constant obtained for the 170 nm BST film, particularly at 500 kHz, demonstrates its potential for applications requiring large capacitance and enhanced charge-storage capability, whereas the 50 nm BST film offers a balanced combination of high dielectric constant and strong voltage tunability suitable for RF and microwave integrated capacitors.

Figure 8 illustrates the dielectric loss (tan δ) as a function of applied bias voltage for the BST thin-film metal–insulator–metal (MIM) capacitors with dielectric thicknesses of 50 nm, 70 nm, and 170 nm, measured over a voltage range of − 20 V to + 30 V at frequencies of 10 kHz, 50 kHz, 500 kHz, and 1 MHz. The dielectric loss is an important parameter that measures the energy lost in the dielectric when an AC system operates. The lower the dielectric loss, the lesser the amount of energy lost and the higher the quality factor **[13], [17]**.

In the case of the 50 nm BST capacitor **(**Fig. 8**(a))**, the dielectric loss remains practically constant in the entire voltage range. In the case of 10 kHz, tan δ changes from about 75 to 100 with an average value of approximately 83. For 50 kHz, the dielectric loss reaches the values from 30 to 32, and for 500 kHz and 1 MHz, it tends towards 1, showing negligible dependence on the voltage. This significant decrease in the dielectric loss at high frequencies means that both interfacial and space charge polarizations have little effect since they are too slow in comparison to the fast alternating electric field **[12],[16]**.

In the case of the 70 nm BST film (Fig. 8(b)), the trend is almost the same but the dielectric loss value at 10 kHz is quite large varying from about 120 to 380 in negative bias but becomes stable to about 190–

200 after the voltage transition. Tan δ at 50 kHz stays almost constant and equal to 75–85 while the dielectric loss at 500 kHz and 1 MHz is close to 1 again. Large oscillations at lower frequencies are explained by the greater role played by the processes of charge trapping, defect assisted conductivity and interfacial polarization in the dielectric material **[12], [18]**.

The BST capacitor of thickness 170 nm **(**Fig. 8**(c))** demonstrates the least regularity in the behavior of the dielectric loss compared to the other two devices. The dielectric loss at 10 kHz is varied between 85 and 120, whereas at 50 kHz, the value changes dramatically from 25 to 130 depending on the level of voltage applied to it. However, the dielectric loss at 500 kHz and 1 MHz is equal to 1. The enhanced fluctuations observed at intermediate frequencies may arise from localized defect states, dielectric relaxation, interface charge trapping, or non-uniform polarization within the thicker BST film **[16], [18].**

Comparison of the three dielectric thicknesses reveals that the dielectric loss is influenced more strongly by measurement frequency than by the applied bias voltage. In all devices, the lowest dielectric loss is consistently observed at 500 kHz and 1 MHz, whereas significantly higher losses occur at 10 kHz and 50 kHz because slow polarization mechanisms, including dipolar, interfacial, and space-charge polarization, contribute substantially to the overall dielectric response at lower frequencies. Furthermore, the nearly constant dielectric loss over the investigated voltage range suggests that the applied electric field has only a limited influence on the intrinsic dielectric dissipation of the BST films. Similar frequency-dependent dielectric-loss behavior has been reported for sputtered BST thin films, where oxygen vacancies, grain boundaries, and interface defects dominate dielectric relaxation and AC conduction processes **[10], [12], [17]**. Therefore, the excellent dielectric-loss characteristics observed at 500 kHz and 1 MHz demonstrate the suitability of the fabricated BST MIM capacitors for high-frequency RF and microwave applications, where minimizing dielectric loss is essential for achieving high quality factors and efficient signal transmission.

Figure 9 presents the calculated electric field–voltage (E–V) characteristics of the BST thin-film metal–insulator–metal (MIM) capacitors with dielectric thicknesses of 50 nm, 70 nm, and 170 nm over the applied bias range of − 20 V to + 30 V. The electric field was determined from the applied voltage using the relation $E = V/d$, where $V$is the applied bias voltage and $d$is the BST dielectric thickness. Since the electric field depends only on the applied voltage and dielectric thickness, all measurement frequencies (10 kHz, 50 kHz, 500 kHz, and 1 MHz) produce identical curves, indicating that the electric field is independent of the excitation frequency.

In the case of the 50 nm BST dielectric **(**Fig. 9**(a))**, the electric field varies linearly with respect to the applied voltage, and has values of about 4.0 MV cm^{-1} at -20 V and 6.0 MV cm^{-1} at + 30 V, tending to be close to zero in the region of zero bias. As the dielectric layer is the thinnest, the 50 nm capacitor has the greatest value of electric field intensity for the applied voltage. High electric fields promote the alignment of polarization in the BST dielectric **[14]**.

As far as the 70 nm BST capacitor **(**Fig. 9**(b))** is concerned, there is a linear relationship between the electric field and the voltage, albeit with smaller values due to the thicker dielectric. The value of the

electric field ranges from about 2.9 MV cm^{-1} at − 20 V to 4.3 MV cm^{-1} at + 30 V. This means that a smaller driving force for dipole rotation and polarization switching takes place, which is in line with the smaller capacitance and dielectric constant measured for this film **[15], [17]**.

The 170 nm BST dielectric shown in **(**Fig. 9**(c))** has the least value of electric field intensity when compared to other three structures. There is a linear increase in electric field intensity ranging from 1.2 MV cm^{-1} at -20 V to 1.8 MV cm^{-1} at + 30 V, with almost zero value near the zero-bias condition. The decrease in electric field intensity with increase in dielectric thickness is due to the inverse relation of electric field to dielectric thickness. Thus, increased thickness of BST film demands higher voltage operation **[18]**.

From the comparison of the three dielectrics' thicknesses, it is evident that there is an inverse relationship between the thickness of the dielectric and the electric field; the largest intensity of electric field is produced by the 50 nm BST film, followed by the 70 nm and 170 nm dielectric thicknesses. The electric field is completely linearly related to the voltage since it is entirely based on the geometrical structure of the device unlike capacitance and conductance. The higher electric field generated within thinner BST films promotes stronger dipole orientation, enhanced dielectric polarization, and greater capacitance modulation, whereas thicker dielectric layers experience lower internal electric fields, leading to reduced electric-field-driven polarization effects **[6], [13], [18]**. These results confirm that dielectric thickness is a critical design parameter for controlling the internal electric field in BST-based MIM capacitors and consequently influences their overall electrical performance in RF and microwave applications.

Figure 10 presents the normalized capacitance–voltage (C/C_o–V) characteristics of the BST thin-film metal–insulator–metal (MIM) capacitors with dielectric thicknesses of 50 nm, 70 nm, and 170 nm, measured over a bias voltage range of − 20 V to + 30 V at frequencies of 10 kHz, 50 kHz, 500 kHz, and 1 MHz. The normalized capacitance was obtained by dividing the measured capacitance by its reference value (C_o), allowing the voltage-dependent capacitance variation of different devices to be compared independently of their absolute capacitance values. In all three devices, the normalized capacitance increases gradually under negative bias and exhibits a sharp transition near 0 V, indicating electric-field-induced polarization and dielectric tuning within the BST dielectric layer **[13], [14]**.

For the 50 nm BST capacitor **(**Fig. 10**(a))**, all four frequency-dependent curves exhibit nearly identical behavior. The normalized capacitance increases gradually from approximately 0.24–0.27 at − 20 V to approximately 0.55–0.60 immediately before the voltage transition. After the transition near 0 V, the normalized capacitance rapidly reaches $C/C_o \approx 1.0$ and remains essentially constant over the positive bias region for all measurement frequencies. The close overlap of the curves indicates excellent frequency stability and highly reproducible voltage-dependent dielectric behavior. Such uniform normalized capacitance characteristics suggest minimal frequency dispersion and stable polarization switching within the thin BST dielectric **[13], [15]**.

Capacitance-voltage characteristics of the 70 nm BST capacitor (Fig. 10(b)) are also similar; however, a higher level of frequency dispersion is observed. When subjected to negative bias, the normalized capacitance rises from about 0.18–0.25 to about 0.50–0.60 in case of − 20V voltage. After this transition, the normalized capacitance remains constant on the levels of 0.85 at 50 kHz, 0.90 at 10 kHz, 0.93 at 500 kHz, and almost 0.98 at 1 MHz. A lower value of the normalized capacitance in comparison to the one of the 50 nm sample could be caused by decreased polarization response of the dielectric material. Nonetheless, relatively stable curves under positive bias indicate a sufficient degree of dielectric stability **[10],[15]**.

The BST capacitor with 170 nm thickness **(**Fig. 10**(c))** displays the most complicated behavior out of the three capacitors. The ratio C/C_0 at frequencies of 10 kHz, 500 kHz, and 1 MHz shows an almost identical pattern to the thinner BST films, ranging from 0.25–0.35 under the negative bias to nearly 1.0 after switching the voltage. Nevertheless, the curve at 50 kHz displays very distinct fluctuations where the ratio C/C_0 ranges from about 0.30 and 3.05 prior to reducing and becoming close to unity under high positive voltage bias. It is presumed that the peculiar peaks are caused by dielectric relaxation, localized charge trapping, interface states, and the instability of transient polarization in the thicker BST film. Such irregular dielectric response was observed previously due to defect assisted polarization and interface charge in BST thin-film capacitors **[12],[16]**.

The analysis of the three thicknesses of the dielectric material shows that for the BST capacitor with 50 nm thickness, there is the highest stability of normalized capacitance behavior, since at all measured frequencies there is an approach of C/C_0 to the value of 1.0 after the voltage switching. For 70 nm thickness, the stability is high as well, but with some dependence on the frequency. However, for the BST capacitor with 170 nm thickness, there are visible oscillations at 50 kHz, which may be caused by the dielectric relaxation process and polarization effects associated with the interfaces. Thus, according to the results of the normalized capacitance measurement, the thinner dielectric film ensures the uniformity of the electric field induced polarization and voltage stability, while the thicker films are characterized by the greater influence of defects and dielectric relaxation. Consequently, the excellent voltage stability observed for the 50 nm BST film demonstrates its suitability for RF and microwave capacitor applications requiring stable capacitance over a wide operating voltage range.

Figure 11 presents the variation of the dielectric constant (ε_r) and dielectric loss ($\tan\delta$) as a function of frequency for the BST thin-film metal–insulator–metal (MIM) capacitors with dielectric thicknesses of 50 nm, 70 nm, and 170 nm. Dielectric properties were derived using capacitance measurements taken at 10 kHz, 50 kHz, 500 kHz, and 1 MHz. From these results, it can be seen that the dielectric constant and dielectric loss are frequency-dependent properties, exhibiting different responses for the three thicknesses of the BST dielectrics. This kind of dependence is typical of ferroelectric BST thin films, where polarization takes place via different processes at various frequencies **[13], [16]**.

The dielectric constant for the BST capacitor having a thickness of 50 nm **(**Fig. 11**(a))** starts to fall from about 345 at 10 kHz to 180 at 50 kHz, thereafter showing a significant rise to almost 420 at 500 kHz and

then falls once again to around 135 at 1 MHz. On the other hand, the dielectric loss shows a continuous fall with increase in the frequency, starting from about 85 at 10 kHz to 30 at 50 kHz and then falls to approximately 2 at 500 kHz and 1 MHz. The fall in dielectric loss shows that there is suppression of interfacial and space charge polarization.

Similar behavior has been found for the 70 nm BST capacitor **(**Fig. 11**(b))**. The dielectric constant starts from around 115 at 10 kHz and falls to 58 at 50 kHz, rises up to almost 185 at 500 kHz, and reduces to about 132 at 1 MHz. Meanwhile, the dielectric loss starts from around 185 at 10 kHz and decreases to 75 at 50 kHz, then comes down to near 1 at 500 kHz and 1 MHz. In comparison with the 50 nm device, the 70 nm film shows smaller values of the dielectric constant in the tested frequency range.

The dielectric constant for the BST capacitor with the thickness of 170 nm **(**Fig. 11**(c))** has the maximum values compared to other capacitors. The dielectric constant falls drastically from about 800 at 10 kHz to about 50 at 50 kHz, and then rises sharply to about 1090 at 500 kHz and falls to about 450 at 1 MHz. The dielectric loss, on the contrary, increases a little from about 105 at 10 kHz to 120 at 50 kHz, then drops abruptly to nearly zero at 500 kHz and 1 MHz. Therefore, the combination of the high value of dielectric constant and dielectric loss at higher frequencies implies the dielectric stability of the thick BST layer at high-frequency excitation.

Comparison between the three dielectric thicknesses shows that the optimal operating frequency for all BST capacitors, which have been fabricated in this study, is 500 kHz where the dielectric constant achieves its peak value whereas the dielectric loss achieves its minimum value. This result may be attributed to frequency-dependent polarization processes in BST dielectrics. At low frequencies, there is a simultaneous contribution of electronic, ionic, dipolar, and interfacial polarizations in the dielectric properties, but charge accumulation at interfaces increases dielectric loss. When the frequency is increased, the slower polarization processes become inactive such as interfacial polarization and space-charge polarization. Thus, dielectric loss decreases whereas faster polarization mechanisms prevail in the dielectric properties **[12]**, **[16]**. Extremely large values of the dielectric constant for the 170 nm film are probably linked to variations in microstructure, crystallinity, grain orientation, and interface quality, rather than thickness, as other reports on optimized thin films and microstructure have indicated similarly enhanced properties **[6], [18]**. Generally speaking, it is evident that optimization of the thickness of the dielectric layer along with the operating frequency plays an important role in achieving maximum dielectric constant with minimized dielectric loss.

Figure 12 presents the capacitance–voltage (C–V) characteristics of the BST thin-film interdigital capacitor (IDC) fabricated on a platinized silicon substrate using a 100 nm BST dielectric layer and Cr/Au (40/200 nm) interdigital electrodes. The electrical characteristics were measured over a bias voltage range of − 20 V to + 20 V at operating frequencies of 100 kHz, 200 kHz, 500 kHz, 700 kHz, and 1 MHz, while the inset shows the corresponding response measured at 100 kHz. The observed capacitance value shows significant dependency on voltage, with its gradual fall for negative bias values, followed by sharp change near 0 V, after which capacitance becomes almost constant with increase of positive bias

value. This clearly proves that the electric field dependent dielectric properties of the BST film are well modulated through the fringing field capacitance in the interdigital structure.

At 100 kHz (inset), the capacitance decreases gradually from approximately − 0.60 × 10^{-9} F at − 20 V to approximately − 1.45 × 10^{-9} F immediately before the voltage transition, followed by a sharp decrease to approximately − 2.55 × 10^{-9} F, where it remains almost constant throughout the positive bias region. Similar voltage-dependent behavior is observed at the higher operating frequencies. At 200 kHz, the capacitance changes from approximately − 1.15 × 10^{-9} F to − 3.60 × 10^{-9} F, while the corresponding stabilized capacitance values at 500 kHz, 700 kHz, and 1 MHz are approximately − 6.65 × 10^{-9} F, − 5.95 × 10^{-9} F, and − 4.05 × 10^{-9} F, respectively. The largest capacitance magnitude is therefore observed at 500 kHz, whereas comparatively smaller capacitance values are obtained at 100–200 kHz and 1 MHz.

The gradual variation of capacitance under negative bias can be attributed to the progressive alignment of electric dipoles and polarization within the BST dielectric, whereas the abrupt transition near zero bias indicates rapid polarization switching under the applied electric field. Unlike the parallel-plate MIM capacitors, the capacitance of the interdigital structure is predominantly governed by fringing electric fields extending through the BST thin film and the surrounding dielectric environment. Consequently, the electric-field distribution is non-uniform and strongly dependent on the interdigital electrode geometry, resulting in a different voltage response compared with conventional MIM capacitors **[2], [19]**.

The frequency dependence of the capacitance further indicates that the BST thin film exhibits frequency-dependent dielectric polarization. The enhanced capacitance observed at 500–700 kHz suggests an optimum operating region where dipolar polarization remains sufficiently responsive while dielectric losses are comparatively reduced. At 1 MHz, the capacitance decreases slightly because slower polarization mechanisms, including interfacial and space-charge polarization, are unable to follow the rapidly alternating electric field, leaving only the faster electronic and ionic polarization mechanisms to contribute to the overall dielectric response **[12], [16]**. Such frequency-dependent behavior has also been reported for BST-based tunable microwave capacitors and varactors, where dielectric relaxation and polarization dynamics govern the capacitance response under alternating electric fields **[13], [19]**.

Overall, the fabricated BST interdigital capacitor exhibits a stable and repeatable voltage-dependent capacitance response over the investigated frequency range. The pronounced capacitance modulation around the zero-bias region together with the relatively stable response under positive bias demonstrates the suitability of the fabricated IDC for tunable RF and microwave passive components, including integrated capacitors, resonators, impedance-matching networks, and sensing applications. Furthermore, comparison with the parallel-plate MIM capacitors presented in the previous sections highlights the significant influence of electrode geometry on the electric-field distribution and capacitance characteristics, emphasizing that interdigital capacitors provide an attractive planar alternative for integrated microwave electronics **[23–24]**.

Figure 13 presents the conductance–voltage (G–V) characteristics of the BST thin-film interdigital capacitor (IDC) fabricated on a platinized silicon substrate using a 100 nm BST dielectric layer and Cr/Au

(40/200 nm) interdigital electrodes. The electrical properties were investigated over a bias voltage range from − 20 V to + 20 V at frequencies of 100 kHz, 200 kHz, 500 kHz, 700 kHz, and 1 MHz, whereas the inset represents the corresponding G-V behavior at 100 kHz frequency. The conductance shows an increasing trend under negative bias and then experiences a steep change around 0 V, followed by almost no change under positive voltages. Such a pattern clearly reveals the effect of an electric field on the charge carriers of the BST material and implies that the electric field plays a major role in the conductivity of the interdigital capacitor in the zero-bias regime **[12], [16]**.

At 100 kHz (inset), the conductance increases from approximately 0.010 S at − 20 V to nearly 0.022 S immediately before the voltage transition and then abruptly increases to approximately 0.040 S, remaining nearly constant for positive bias voltages. Similar voltage-dependent characteristics are observed at higher frequencies. At 200 kHz, the conductance increases from approximately 0.013 S under negative bias to approximately 0.042 S after the voltage transition. The corresponding conductance values stabilize at approximately 0.038 S for 500 kHz, 0.028 S for 700 kHz, and 0.016 S for 1 MHz. These results indicate that the maximum conductance is obtained at 200 kHz, whereas the minimum conductance is consistently observed at 1 MHz **[25], [26]**.

The gradual increase in conductance under negative bias is attributed to the progressive enhancement of charge-carrier transport and polarization within the BST dielectric as the applied electric field increases. The abrupt increase near 0 V indicates a transition to a higher-conductance state, which may result from increased carrier mobility and the alignment of polarization under the applied electric field. Unlike conventional MIM capacitors, the electrical conduction in the interdigital capacitor is governed primarily by fringing electric fields, which extend laterally through the BST thin film and produce a non-uniform electric-field distribution between adjacent electrodes. Consequently, the voltage dependence of conductance is influenced not only by the dielectric properties of BST but also by the interdigital electrode geometry and electric-field distribution **[2], [19]**.

The conductance values decrease gradually with an increase in frequency, especially beyond 500 kHz when the conductance values are considerably smaller than those measured at 200 kHz. This is due to the fact that the slower processes such as interfacial polarization and space charge polarization become less effective at higher frequencies due to the rapid variation of the electric field which does not allow the charge carriers to follow. In consequence, only faster processes, i.e. electronic and ionic polarization play a role in the AC conduction, which results in low conductance at 700 kHz and 1 MHz **[12], [16]**. The same frequency dependence of the conductance values has been reported for the sputtered BST thin films and tunable microwave dielectric devices **[13], [17]**.

In summary, the fabricated BST-based IDC shows stable conductance behavior in the measured voltage range with distinct behavior at around 0 V and low conductance at higher frequencies. The low conductance value recorded at 1 MHz demonstrates low dielectric loss, thereby showing the suitability of the fabricated IDC for use in radio frequency and microwave integrated passive devices. On the other

hand, the conduction behavior is different from the one exhibited by the BST-based MIM capacitors, since the IDC structure uses the interdigital field distribution.

The frequency dependence of capacitance of the BST thin film interdigital capacitor (IDC) created on a platinized silicon substrate, with the dielectric layer of BST with thickness 100 nm and Cr/Au (40/200 nm) interdigital electrodes, is shown in **(**Fig. 14**)**. The measurements were performed within the frequency range from 100 kHz to 1 MHz, for the following applied bias voltages 5 V, 10 V, 15 V, 20 V, and 30 V. It can be seen from the results that the capacitance of the studied capacitor shows strong frequency dependence but at the same time it is quite insensitive to the change of the applied bias voltage, which is clearly illustrated by overlapping of all five voltage dependences in the whole frequency range **[13], [16]**.

For all bias voltages, the measured capacitance declines steadily from about -2.5×10^{-9} F at 100 kHz to a minimum value of about -6.5×10^{-9} F near 500 kHz. Above this point, the measured capacitance begins to increase steadily to about -4.0×10^{-9} F at 1 MHz. The variation among the five graphs obtained at 5 V, 10 V, 15 V, 20 V, and 30 V is negligible, which suggests that the effect of the bias voltage on the total capacitance is rather insignificant in the measured frequency range **[18], [19]**.

The obtained non-monotonic dielectric response is related to the frequency-dependent dielectric relaxation in the BST thin-film layer. In the low-frequency region, all four mentioned polarization mechanisms are active in providing the total dielectric response; therefore, the measured capacitance values are rather high **[20]**. As the frequency approaches 500 kHz, the slower processes such as the interfacial and space charge polarizations cannot follow the alternating electrical field anymore, and thus, the measured minimum of capacitance is observed. The higher frequency corresponds to the domination of the electronic and ionic polarization mechanisms and causes the increase in the measured capacitance value up to 1 MHz. Such kind of dielectric relaxation behavior has been observed for BST thin films and ferroelectric microwave capacitors at the same frequency range **[12], [13], [19]**.

Further, the very slight dependency of the capacitance value upon the DC bias also implies that the electric field distribution due to the fringing effect within the interdigital capacitor electrode configuration is stable over the whole investigated voltage range. Indeed, the capacitance value of the interdigital capacitor is defined by the fringing electric fields, not by the parallel plate electric field. Therefore, the obtained response shows the effect of the interdigital electrode structure along with the dielectric properties of the BST thin film **[27], [28]**.

All in all, the frequency stability of the obtained response along with the low voltage dependency is shown. Hence, it can be stated that the fabricated BST thin-film interdigital capacitor demonstrates good frequency stability together with the minimal voltage dependency. The stable response and dielectric performance show that the proposed IDC design can be successfully used as a part of tunable RF and microwave passive devices **[29], [30]**.

Figure 15 shows the frequency dependence of the conductance of the BST thin-film interdigital capacitor (IDC) grown on a platinized silicon substrate with a 100 nm BST dielectric layer and Cr/Au (40/200 nm) interdigital electrodes. The conductance measurements were carried out at the frequencies from 100 kHz to 1 MHz for the following values of applied bias voltages: 5 V, 10 V, 15 V, 20 V, and 30 V. It is clearly seen that the conductance shows significant frequency dependence, while the effect of applied bias voltage can be considered to be negligible, since all five voltage dependence curves almost entirely coincide in the whole investigated frequency range **[33]**.

In all cases, there is an increase in conductance with the increase in frequency up to the point when its value reaches approximately 0.0422 S at 300 kHz. Above this frequency, there is a continuous decrease in conductance with an increase in frequency up to 1 MHz where it is about 0.017 S.The nearly identical conductance values obtained at 5 V, 10 V, 15 V, 20 V, and 30 V demonstrate excellent electrical stability and indicate that the conduction mechanism is essentially independent of the applied bias within the investigated operating range **[31–32]**.

The initial increase in conductance observed between 100 kHz and 300 kHz can be attributed to enhanced AC charge transport resulting from the effective response of dipolar and interfacial polarization mechanisms under moderate excitation frequencies. As the operating frequency increases further, these slower polarization mechanisms are no longer able to follow the rapidly alternating electric field, causing a progressive reduction in charge transport and, consequently, a decrease in conductance **[34]**. At higher frequencies, the electrical response becomes dominated by the faster electronic and ionic polarization processes, which contribute less to AC conduction than interfacial and space-charge polarization **[12], [16]**. Similar frequency-dependent conductance behavior has been reported for BST thin films and ferroelectric dielectric materials, where dielectric relaxation and defect-assisted charge transport govern the AC electrical response **[13], [17]**.

The absence of noticeable voltage dependence indicates that the fringing electric-field distribution within the interdigital electrode structure remains stable over the applied bias range. Unlike conventional metal–insulator–metal capacitors, where current transport occurs predominantly through the dielectric thickness, the conductance of the interdigital capacitor is strongly influenced by lateral fringing electric fields between adjacent electrodes. Consequently, the observed frequency response reflects the combined effects of dielectric relaxation, charge transport within the BST layer, and the interdigital electrode geometry **[2], [19]**.

Overall, the fabricated BST thin-film interdigital capacitor exhibits stable conductance characteristics over a wide frequency range, with a maximum conductance near 300 kHz followed by a gradual reduction toward 1 MHz. Low values of the conductance at high frequencies reflect low AC conductivity and reduced loss of dielectric energy, which is favorable for RF and microwave passive devices. It can be seen from the presented data that the investigated BST thin film IDC possesses reliable high-frequency electrical properties to be used in microwave circuits, tunable capacitance, impedance matching, and sensors **[35], [36]**.

4. Conclusion

A comparative study involving fabrication of MIM capacitors using BST thin film with dielectric thickness of 50 nm, 70 nm, and 170 nm and IDC capacitors with a dielectric thickness of 100 nm BST material has been carried out to investigate the effect of dielectric thickness and device geometry on the electrical performance. All the capacitors have been fabricated on platinized Si substrate using radio-frequency magnetron sputtering technique for BST film deposition and thermal evaporation method for electrode deposition.

The experimental results demonstrate that dielectric thickness plays a significant role in determining the electrical characteristics of BST MIM capacitors. Among the fabricated devices, the 50 nm BST capacitor exhibited the highest capacitance density (≈ 0.074 F m^{-2}), the highest quality factor (≈ 3.1 at 1 MHz), and the maximum electric field (≈ 6 MV cm^{-1}), indicating superior charge-storage capability and reduced dielectric loss. In contrast, the 170 nm BST capacitor exhibited the highest dielectric constant (≈ 1090 at 500 kHz), suggesting that microstructural characteristics together with dielectric thickness contribute to the enhanced dielectric response. In all MIM capacitors, dielectric loss decreased with increasing frequency, while stable conductance and normalized capacitance characteristics confirmed reliable electrical performance over the investigated operating conditions.

The fabricated 100 nm BST interdigital capacitor exhibited stable capacitance and conductance characteristics with only minor variations under different applied bias voltages. Its frequency-dependent electrical response confirms that the fringing electric-field distribution associated with the interdigital geometry provides stable operation over the investigated frequency range, making it suitable for planar integrated passive components.

Overall, the present work demonstrates that both dielectric thickness and capacitor geometry are critical design parameters for optimizing BST thin-film capacitors. Thin BST dielectrics are preferable for applications requiring high capacitance density and low-loss operation, whereas thicker BST films are advantageous where high dielectric permittivity is desired. The findings provide a practical basis for the development of high-performance BST thin-film capacitors for next-generation RF, microwave, tunable electronic, and integrated passive device applications.

Declarations

CRediT authorship contribution statement

Abdullah: Conceptualization, Methodology, Investigation, Formal analysis, Data curation, Validation, Visualization, Writing – original draft, Writing – review & editing, Resources.

Declaration of competing interest

The author declares that there are no known competing financial interests or personal relationships that could have appeared to influence the work reported in this paper.

Acknowledgement

The authors thank Prof. Mahesh Kumar and the Central Research Facility (CRF), IIT Jodhpur, for providing access to the facilities and instruments used in this research.

Data availability. Data will be made available on request.

References

1. **1.** S. N. Arinze and A. O. Nwajana, “A Comprehensive Review of Battery-Free Energy Efficient RF and Microwave Systems,” *Journal of Engineering*, vol. 2026, Art. no. 4227736, 2026, **doi: 10.1155/je/4227736.**
2. **2.** R. R. Mansour, G. Basavarajappa, and S. M. Pourjaafari, “High-Q Tunable Bandpass Filters With a Wide Tuning Range Using a Minimum Number of Tuning Elements,” *IEEE Microwave Magazine*, vol. 27, no. 7, pp. 14–29, Jul. 2026, **doi: 10.1109/MMM.2025.3572869.**
3. **3.** R. Gomez-Garcia, L. Yang, M. Malki, N. Iranpour, J. D. Ang, Z. Luo, X.-B. Zhao, S. Wang, R. Li, J.-M. Muñoz-Ferreras, and X. Zhu, “Reflectionless Design in RF Passive and Active Circuits: Recent Advances and Emerging Trends,” *IEEE Transactions on Circuits and Systems I: Regular Papers*, vol. 73, no. 7, pp. 4482–4495, Jul. 2026, doi: 10.1109/TCSI.2026.3667828.
4. **4.** H. Tan, Y. Deng, K. Li, Y. Wu, F. He, L. Yang, G. Zhang, and X. Wang, “Ultra-high energy storage of nanocrystalline strontium-modified barium titanate with paraelectric properties,” *Ceramics International*, vol. 52, pp. 31984–31991, 2026, doi: 10.1016/j.ceramint.2026.05.240.
5. **5.** C. Ribeiro, A. Tkach, J. Noudem, C. Randall, M. E. Costa, and P. M. Vilarinho, “Grain-boundary engineering by spark plasma texturing to enhance dielectric breakdown strength in barium strontium titanate ceramics,” *Chemical Engineering Journal*, vol. 535, Art. no. 175499, 2026, doi: 10.1016/j.cej.2026.175499.
6. **6.** G. Kaur, S. Mantri, F. Liu, *et al.*, “Phase Boundary Enabled High Dielectric Tunability in $Ba_{1-x}Sr_xTiO_3$ Thin Films and their Integration on Silicon,” *Advanced Materials*, vol. 38, Art. no. e73172, 2026, **doi: 10.1002/adma.73172.**
7. **7.** S. Jafarpour, S. R. Hosseini, and H. Naghshara, “Ta doping-induced enhancement of dielectric performance in sputtered $BaTiO_3$ thin films for MIM capacitors,” *Physica Scripta*, vol. 101, no. 6, Art. no. 065905, 2026, doi: 10.1088/1402-4896/ae32d4.
8. **8.** M. Chaudhary, S. Jindal, S. Devi, and S. Kaur, “Optimizing Structural, Optical, and Magnetic Properties of $Ba_{0.92}Sr_{0.08}Ti_{1-x}Cr_xO_3$ Ceramics for Multifunctional Applications,” *Journal of Electronic Materials*, vol. 55, pp. 136–143, 2026, doi: 10.1007/s11664-025-12503-4.
9. **9.** F. Bergmann, M. R. Barone, Z. Tian, *et al.*, “Breaking symmetry yields a low-loss out-of-plane tunable microwave dielectric,” *Nature Electronics*, 2026, doi: 10.1038/s41928-026-01651-y.
10. **10.** B. G. Thali, D. S. Agrahari, and R. M. Kamble, “Fabrication of barium strontium titanate encapsulated with graphene nanosheets for bifunctional sensor and energy storage application,”

Electrochimica Acta, vol. 551, Art. no. 148196, 2026, doi: 10.1016/j.electacta.2026.148196.

11. **11.** B. Jasim and M. Kaleli, “Electrode material influence on thin film BST ceramic capacitor,” *Applied Physics A*, vol. 132, Art. no. 142, 2026, doi: 10.1007/s00339-026-09335-2.
12. **12.** F. El Kamel, Z. Ben Cheikh, and O.-G. Lavallée, “Dielectric Properties of Amorphous ($Ba_{2}/_{3}$,$Sr_{1}/_{3}$)TiO_3 Films,” *Journal of the American Ceramic Society*, vol. 109, Art. no. e70924, 2026, **doi: 10.1111/jace.70924.**
13. **13.** M. Chaudhary, S. Jindal, S. Devi, and S. Kaur, “Optimizing Structural, Optical, and Magnetic Properties of $Ba_{0.92}Sr_{0.08}Ti_{1-}CrO_3$ Ceramics for Multifunctional Applications,” *Journal of Electronic Materials*, vol. 55, pp. 136–143, 2026, **doi: 10.1007/s11664-025-12503-4.**
14. **14.** G. Deng, H. Hao, Z. Yao, M. Cao, and H. Liu, “Grain Size Effect on the Dielectric Property of $Ba_{0.5}Sr_{0.5}TiO_3$ Ceramic/Barium Boroaluminosilicate Glass Composites,” *Journal of Materials Research*, 2026, **doi: 10.1557/s43578-026-01838-1.**
15. **15.** T. P. Mach, L. Huang, N. R. M. D. Ashif, U. Gengenbach, and J. R. Binder, “Inkjet Printed Tunable BST/P(VDF-TrFE) Dielectrics on Polymeric Substrates for Varactor Applications,” *Advanced Composites and Hybrid Materials*, vol. 9, Art. no. 81, 2026, doi: 10.1007/s42114-026-01628-7.
16. **16.** M. Zhang, R. Zhu, X. Chen, X. Yu, Z. Zhang, and Z. Wang, “A-site Entropy-Engineered BST-Based Dielectric Films with High Dielectric Tunability and Excellent Thermal Stability,” *Journal of the European Ceramic Society*, vol. 46, Art. no. 118415, 2026, **doi: 10.1016/j.jeurceramsoc.2026.118415.**
17. **17.** G. Kaur, S. Mantri, F. Liu, S. Hazra, S. Chen, Y. Si, *et al*., “Phase Boundary Enabled High Dielectric Tunability in Ba_{1-}SrTiO_3 Thin Films and Their Integration on Silicon,” *Advanced Materials*, vol. 38, Art. no. e73172, 2026, **doi: 10.1002/adma.73172.**
18. **18.** B. Jasim and M. Kaleli, “Electrode Material Influence on Thin Film BST Ceramic Capacitor,” *Applied Physics A*, vol. 132, Art. no. 142, 2026, **doi: 10.1007/s00339-026-09335-2.**
19. **19.** X. Zhang, W. Li, S. Yu, X. Fan, X. Wang, H. Li, J. Song, X. Li, and X. Zhang, “Thickness-Driven Microstructure Evolution and Domain Wall Enhanced Energy Storage in Epitaxial $Ba_{0.6}Sr_{0.4}TiO_3$ Ferroelectric Films,” *Journal of Materials Science: Materials in Electronics*, vol. 37, Art. no. 144, 2026, **doi: 10.1007/s10854-026-16583-8.**
20. **20.** S. Subhash, S. Kooriyattil, T. S. Akhil Raman, S. Shyam Shankar, and K. C. James Raju, “Enhanced Charge Storage and Ferroelectric-Like Switching in PLD-Grown $Zn_{0.85}Mg_{0.15}O$ MIM Capacitors via Thickness Engineering for Non-Volatile Memory Devices,” *Journal of Materials Science: Materials in Electronics*, vol. 37, Art. no. 1409, 2026, **doi: 10.1007/s10854-026-17819-3.**
21. **21.** G. Deng, H. Hao, Z. Yao, M. Cao, and H. Liu, “Grain Size Effect on the Dielectric Property of $Ba_{0.5}Sr_{0.5}TiO_3$ Ceramic/Barium Boroaluminosilicate Glass Composites,” *Journal of Materials Research*, 2026, **doi: 10.1557/s43578-026-01838-1.**
22. **22.** R. Chang, Z. Yao, H. Hao, M. Cao, and H. Liu, “Strategic Optimization of DC Bias Stability in $BaTiO_3$ Ceramics Through Defect-Engineered Core-Shell Architectures,” *Journal of Materiomics*, vol. 12, Art. no. 101216, 2026, **doi: 10.1016/j.jmat.2026.101216.**

23. **23.** N. Al Meselmene, P. Agarwal, J. Fu, K. V. Sreekanth, S. L. Teo, A. J. Sim, K. L. Ke, P. Yang, A. Nemati, E. Dogheche, and J. Teng, “Barium Strontium Titanate Thin Film for Electrically Tunable THz Metasurface,” *Small Structures*, vol. 7, Art. no. e202500339, 2026, **doi: 10.1002/sstr.202500339.**
24. **24.** K. E. Ibrahim and H. A. Kassim, “Synthesis and Characterization of $SrTiO_3$–Hydroxyapatite Composite Ceramics Prepared by Microwave-Assisted Sintering for Electro-Active Biomedical Applications,” *Ceramics–Silikáty*, vol. 70, no. 2, pp. 275–281, 2026, **doi: 10.13168/cs.2026.0016.**
25. **25.** S. W. Kirchoefer, E. J. Cukauskas, N. S. Barker, H. S. Newman, and W. Chang, “Barium–strontium–titanate thin films for application in radio-frequency-microelectromechanical capacitive switches,” *Applied Physics Letters*, vol. 80, no. 7, pp. 1255–1257, Feb. 2002, **doi: 10.1063/1.1450263.**
26. **26.** V. M. Mukhortov, S. V. Biryukov, Y. I. Golovko, and S. I. Masychev, “Effect of the Polarization of Nanosized Barium Strontium Titanate Films on the Characteristics of Ferroelectric Microwave Phase Shifters,” *Bulletin of the Russian Academy of Sciences: Physics*, vol. 88, no. 5, pp. 677–681, 2024, **doi: 10.1134/S1062873824706408.**
27. **27.** X. Wei, K. Deng, A. Gong, Z. Zhang, Z. Zhou, L. Sang, B. Zhang, Q. Zhang, and W. Huang, “Adjustable Ultra-high Density Capacitor Based on Self-rolled-up Technology,” in *Proc. 2024 International Conference on Microwave and Millimeter Wave Technology (ICMMT)*, 2024, **doi: 10.1109/ICMMT61774.2024.10672245.**
28. **28.** R. G. Bovadilla, G. P. Rehder, G. Griep, A. L. C. Serrano, and L. G. Gomes, “3D Interdigital Capacitors Based on the MnM Interposer for mm-Wave Applications,” in *Proc. 2025 SBMO/IEEE MTT-S International Microwave and Optoelectronics Conference (IMOC)*, 2025, pp. 820–824, **doi: 10.1109/IMOC65414.2025.11365836.**
29. **29.** W. Zhu, L. Wang, Y. Chen, and H. Chen, “Research on the Substitution of MIM Capacitors and MOM Capacitors on 12-Inch 90-nm BCD Process,” in *Proc. 2024 Conference of Science and Technology for Integrated Circuits (CSTIC)*, 2024, **doi: 10.1109/CSTIC61820.2024.10532093.**
30. **30.** A. Bharti, V. Niranjan, B. Bhardwaj, S. Keisham, R. Yadav, and K. Duggal, “Review Paper of Metal Insulator Metal and Metal Oxide Metal Capacitors for Improved Capacitance and Overall Performance,” in *Proc. 2024 International Conference on Signal Processing and Advance Research in Computing (SPARC)*, 2024, **doi: 10.1109/SPARC61891.2024.10829176.**
31. **31.** S. Zhao, Z. Ran, Y. Yang, J. Chen, and Y. Huang, “On-Chip Femtofarad Capacitance Standard Based on Interdigital Structure,” *IEEE Transactions on Instrumentation and Measurement*, vol. 74, Art. no. 1507808, 2025, **doi: 10.1109/TIM.2025.3612646.**
32. **32.** M.-M. Laurila, K. Lozano Montero, and M. Mäntysalo, “A Combination of Experimental and Numerical Method for Optimizing the Sensitivity of Ultra-Thin Piezoelectric Sensor With Interdigitated Electrodes,” *Flexible and Printed Electronics*, vol. 8, no. 1, Art. no. 015006, 2023, **doi: 10.1088/2058-8585/acb36b.**
33. **33.** J. P. Goud, A. Kumar, M. S. Alkathy, K. Sandeep, A. Raman T. S., B. Sahoo, J. Ryu, and K. C. James Raju, “Thickness Dependence of Microwave Dielectric Tunability in $Ba_{0.5}Sr_{0.5}TiO_3$ Thin Films

Deposited by Pulsed Laser Deposition," *Ceramics International*, vol. 49, no. 1, pp. 1188–1194, 2023, **doi: 10.1016/j.ceramint.2022.09.095.**

34. **34.** C. Huo, X. Zhang, C. Li, H. Xu, P. Yu, L. Cheng, C. Zheng, and Z. Gu, "Robust Tunability and Newly Emerged Q Resonance of $Ba_{0.8}Sr_{0.2}TiO_3$-Based Microwave Capacitors under Gamma Irradiations," *ACS Applied Materials & Interfaces*, vol. 16, pp. 23517–23524, 2024, **doi: 10.1021/acsami.3c19131.**
35. **35.** R. G. Aredes, E. Antonelli, L. P. Silva Neto, J. O. Rossi, G. N. Lima, J. J. Barroso, E. G. L. Rangel, and E. Schamiloglu, "Development of Tunable Ferroelectric Ceramic Capacitors," *IEEE Transactions on Ultrasonics, Ferroelectrics, and Frequency Control*, vol. 70, no. 8, pp. 885–894, Aug. 2023, **doi: 10.1109/TUFFC.2023.3282625.**
36. **36.** R. Sapawi, K. Kipli, N. Julai, K. H. Ping, S. A. Z. Murad, and D. N. S. Awg Salleh, "A 0.89 to 2.1 GHz Tunable Power Amplifier for Multi-band Transmitter," in *Proc. 12th International Conference on Power Science and Engineering (ICPSE)*, 2023, pp. 91–96, **doi: 10.1109/ICPSE59506.2023.10329295.**

Figures

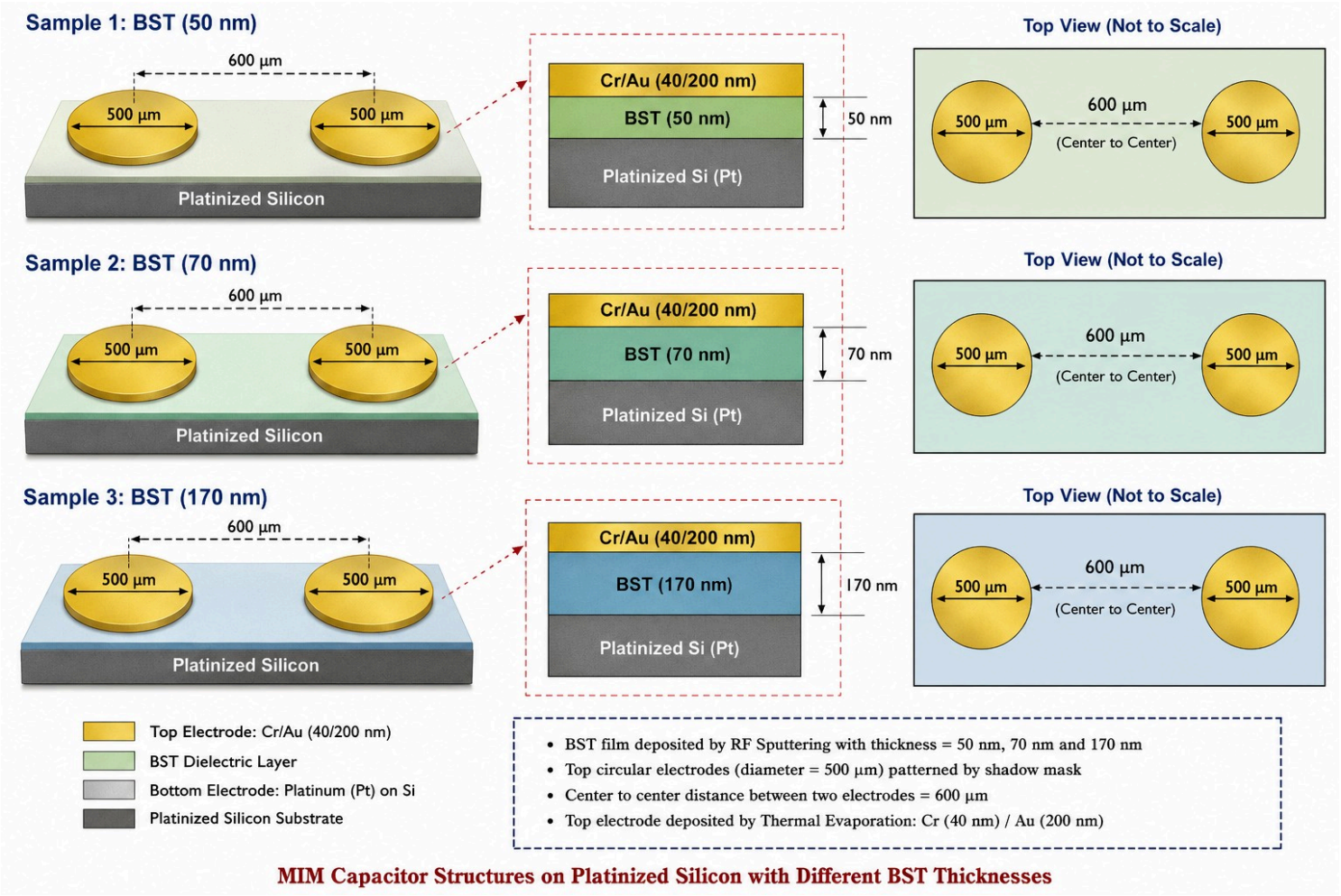


Figure 1

Schematic representation of BST-based MIM capacitor devices fabricated on platinized silicon substrates with dielectric thicknesses of 50, 70, and 170 nm, employing Cr/Au (40/200 nm) circular top electrodes (500 µm diameter) separated by a center-to-center distance of 600 µm.

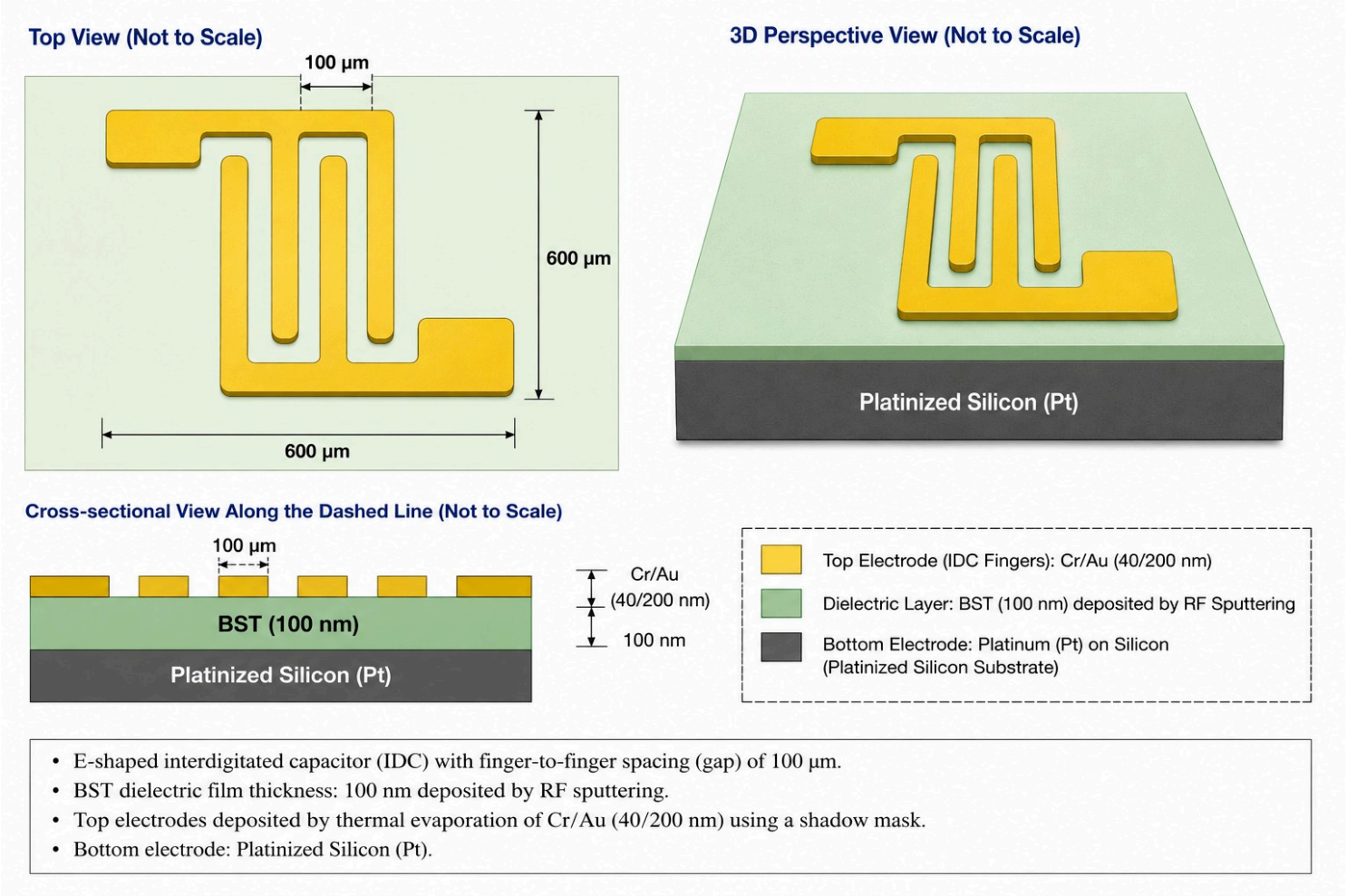


Figure 2

Schematic illustration of the BST-based interdigital capacitor (IDC) fabricated on a platinized silicon substrate. The device comprises a 100 nm BST dielectric film deposited by RF sputtering, with Cr/Au (40/200 nm) interdigital electrodes patterned on the dielectric layer by thermal evaporation through a shadow mask. The interdigital electrode geometry employs an E-shaped finger configuration with a constant inter-finger spacing of 100 µm. The figure includes the top-view electrode pattern, three-dimensional schematic, and cross-sectional view of the device architecture.

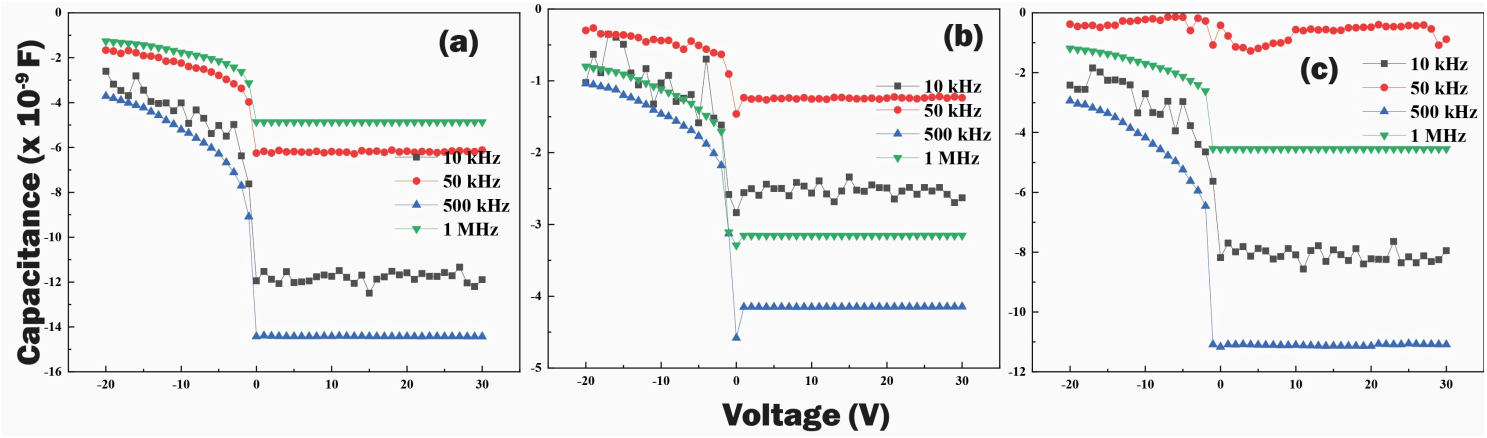


Figure 3

Capacitance–voltage (C–V) characteristics of metal–insulator–metal capacitors fabricated on a platinized silicon substrate with circular chromium/gold (40 nm/200 nm) top electrodes and barium strontium titanate dielectric films of varying thicknesses: **(a)** 50 nm, **(b)** 70 nm, and **(c)** 170 nm. The C–V characteristics were measured over a bias voltage range of −20 V to +30 V at frequencies of 10 kHz, 50 kHz, 500 kHz, and 1 MHz.

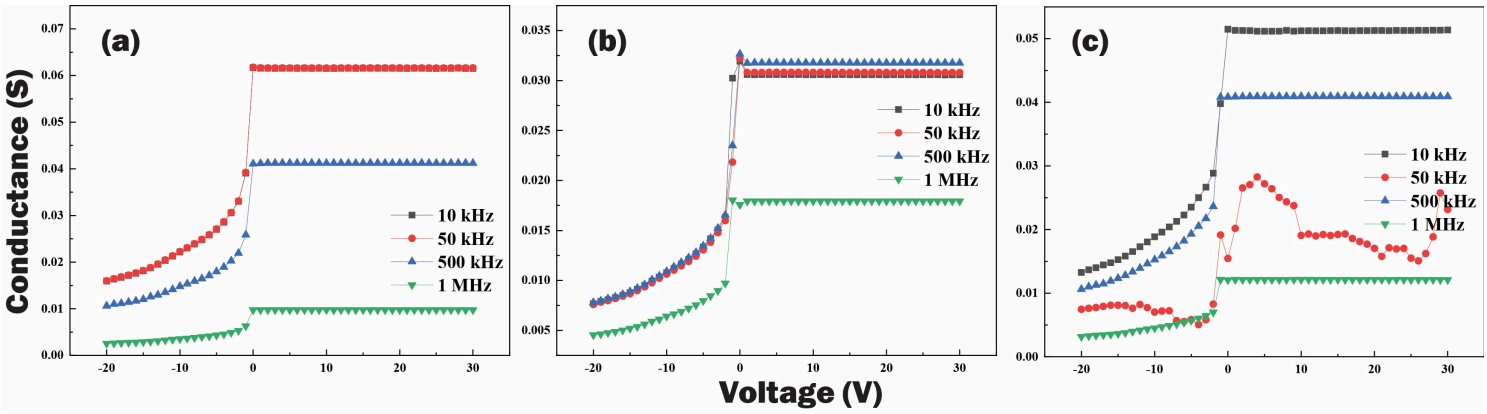


Figure 4

Conductance–voltage (G–V) characteristics of metal–insulator–metal capacitors fabricated on a platinized silicon substrate with circular chromium/gold (40 nm/200 nm) top electrodes and barium strontium titanate dielectric films of varying thicknesses: **(a)** 50 nm, **(b)** 70 nm, and **(c)** 170 nm. The G–V characteristics were measured over a bias voltage range of −20 V to +30 V at frequencies of 10 kHz, 50 kHz, 500 kHz, and 1 MHz.

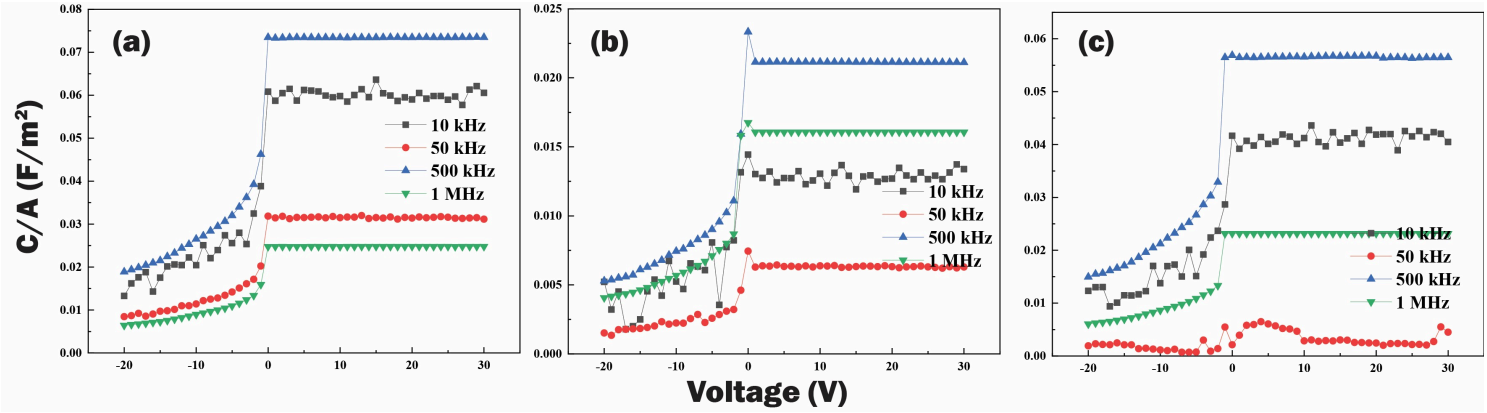


Figure 5

Capacitance density–voltage (C/A_V) characteristics of metal–insulator–metal capacitors fabricated on a platinized silicon substrate with circular chromium/gold (40 nm/200 nm) top electrodes and barium strontium titanate dielectric films of varying thicknesses: **(a)** 50 nm, **(b)**70 nm, and **(c)** 170 nm. The capacitance density $(C/A,\ \mathrm{F/m^2})$was measured over a bias voltage range of −20 V to +30 V at frequencies of 10 kHz, 50 kHz, 500 kHz, and 1 MHz.

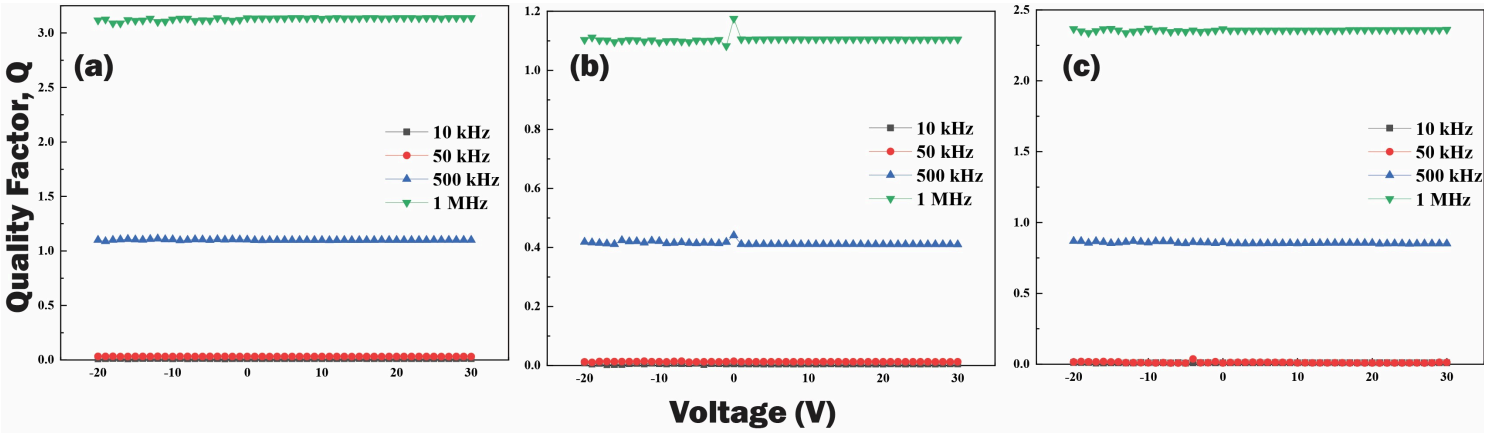


Figure 6

Quality factor (Q-factor)–voltage (Q–V) characteristics of metal–insulator–metal capacitors fabricated on a platinized silicon substrate with circular chromium/gold (40 nm/200 nm) top electrodes and barium strontium titanate dielectric films of varying thicknesses: **(a)** 50 nm, **(b)** 70 nm, and **(c)** 170 nm. The Q-factor was measured over a bias voltage range of −20 V to +30 V at frequencies of 10 kHz, 50 kHz, 500 kHz, and 1 MHz.

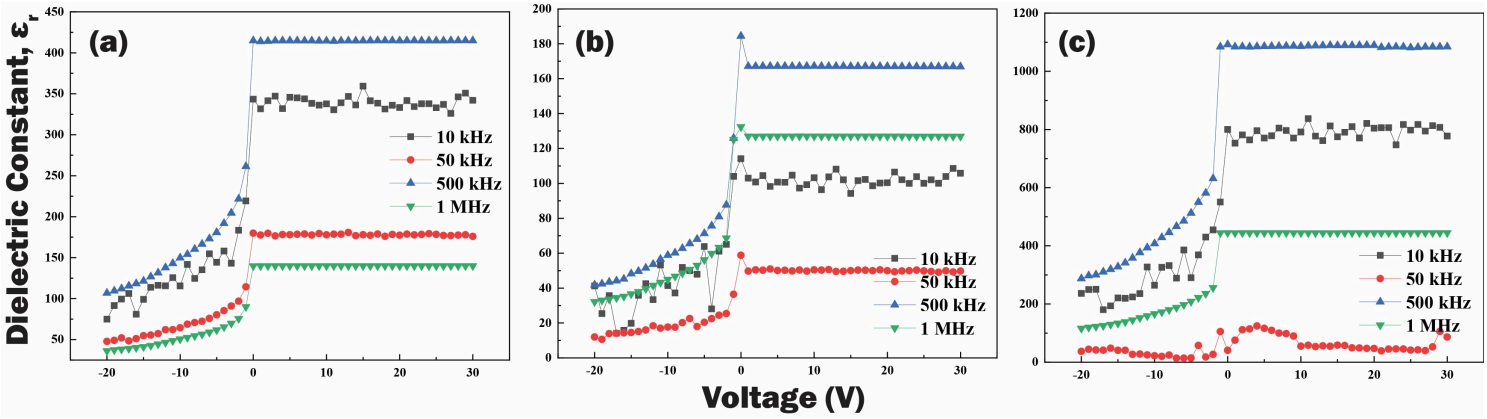


Figure 7

Dielectric constant–voltage $(\varepsilon_r – V)$ characteristics of metal–insulator–metal capacitors fabricated on a platinized silicon substrate with circular chromium/gold (40 nm/200 nm) top electrodes and barium strontium titanate dielectric films of varying thicknesses: **(a)** 50 nm, **(b)** 70 nm, and **(c)** 170 nm. The dielectric constant was extracted from the measured capacitance over a bias voltage range of −20 V to +30 V at frequencies of 10 kHz, 50 kHz, 500 kHz, and 1 MHz.

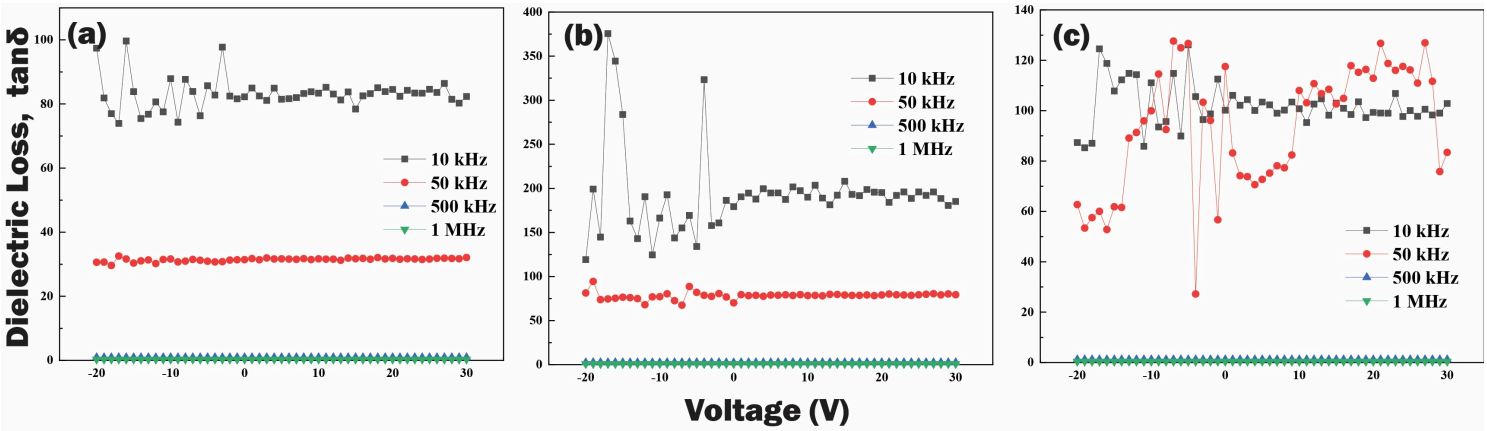


Figure 8

Dielectric loss (tan δ)–voltage characteristics of metal–insulator–metal capacitors fabricated on a platinized silicon substrate with circular chromium/gold (40 nm/200 nm) top electrodes and barium strontium titanate dielectric films of varying thicknesses: **(a)** 50 nm, **(b)** 70 nm, and **(c)** 170 nm. The dielectric loss (tan δ) was measured over a bias voltage range of −20 V to +30 V at frequencies of 10 kHz, 50 kHz, 500 kHz, and 1 MHz.

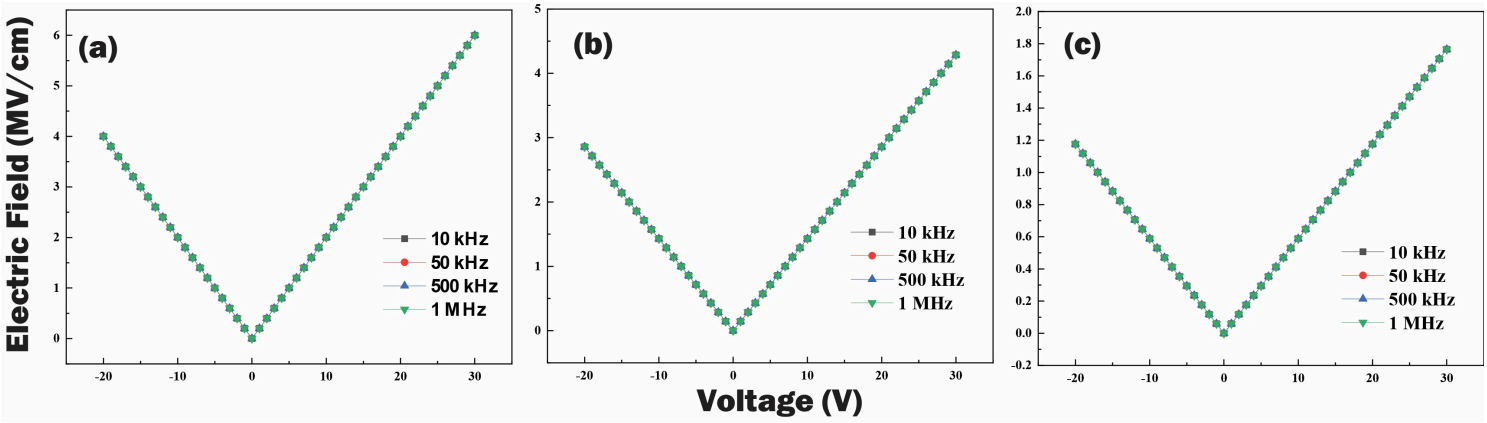


Figure 9

Electric field–voltage (E–V) characteristics of metal–insulator–metal capacitors fabricated on a platinized silicon substrate with circular chromium/gold (40 nm/200 nm) top electrodes and barium strontium titanate dielectric films of varying thicknesses: **(a)** 50 nm, **(b)** 70 nm, and **(c)** 170 nm. The electric field was calculated from the applied bias voltage over a voltage range of −20 V to +30 V.

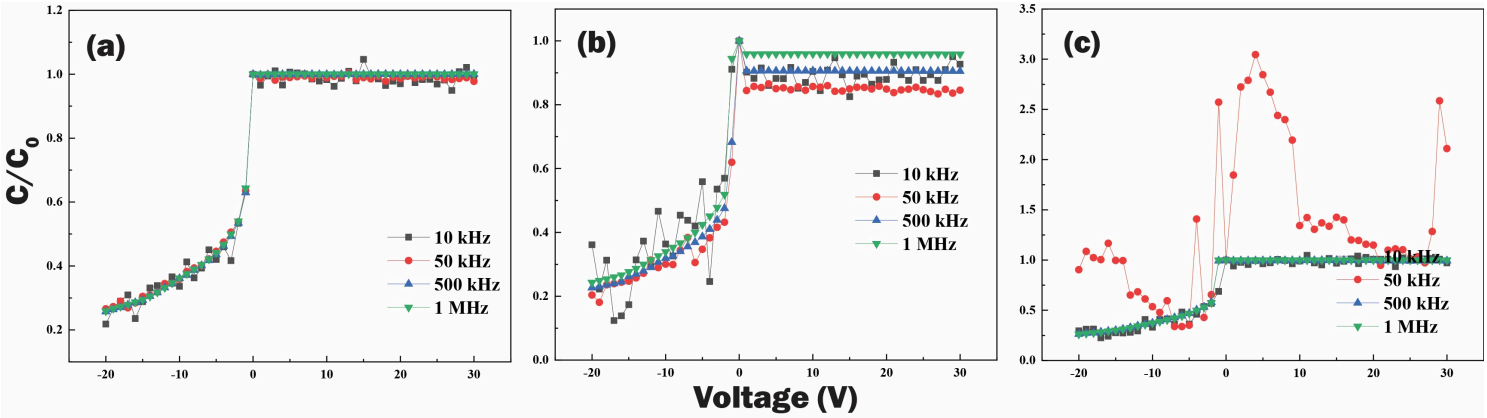


Figure 10

Normalized capacitance–voltage $(C/C_0–V)$characteristics of metal–insulator–metal capacitors fabricated on a platinized silicon substrate with circular chromium/gold (40 nm/200 nm) top electrodes and barium strontium titanate dielectric films of varying thicknesses: **(a)** 50 nm, **(b)** 70 nm, and **(c)** 170 nm. The normalized capacitance $(C/C_0)$was obtained from the measured capacitance over a bias voltage range of −20 V to +30 V at frequencies of 10 kHz, 50 kHz, 500 kHz, and 1 MHz.

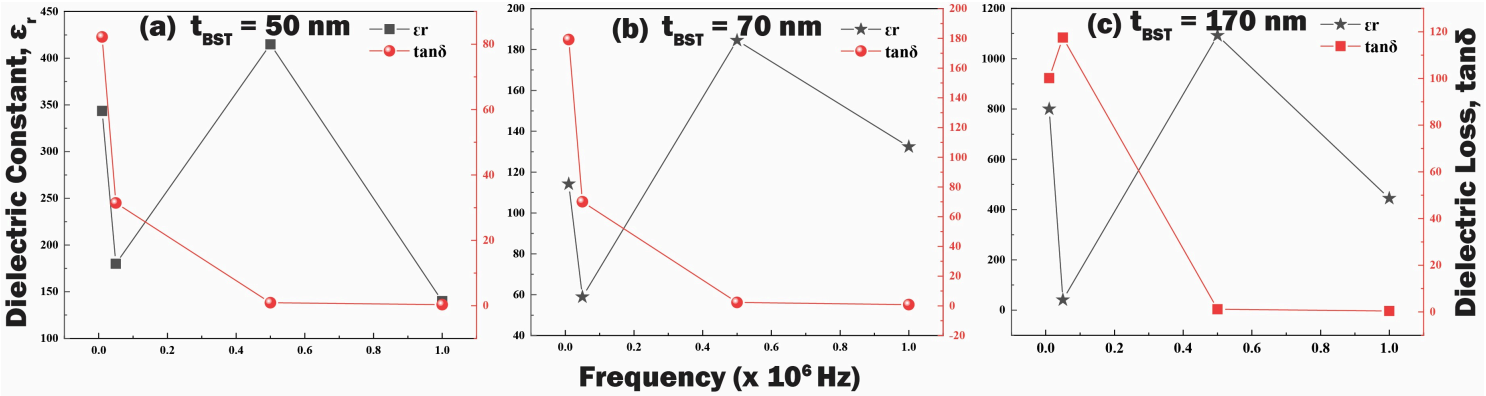


Figure 11

Variation of dielectric constant $(\varepsilon_r)$and dielectric loss $(\tan\delta)$as a function of frequency for metal–insulator–metal capacitors fabricated on a platinized silicon substrate with circular chromium/gold (40 nm/200 nm) top electrodes and barium strontium titanate dielectric films of different thicknesses: **(a)** 50 nm, **(b)**70 nm, and **(c)** 170 nm. The dielectric constant and dielectric loss were extracted from capacitance measurements performed at frequencies of 10 kHz, 50 kHz, 500 kHz, and 1 MHz.

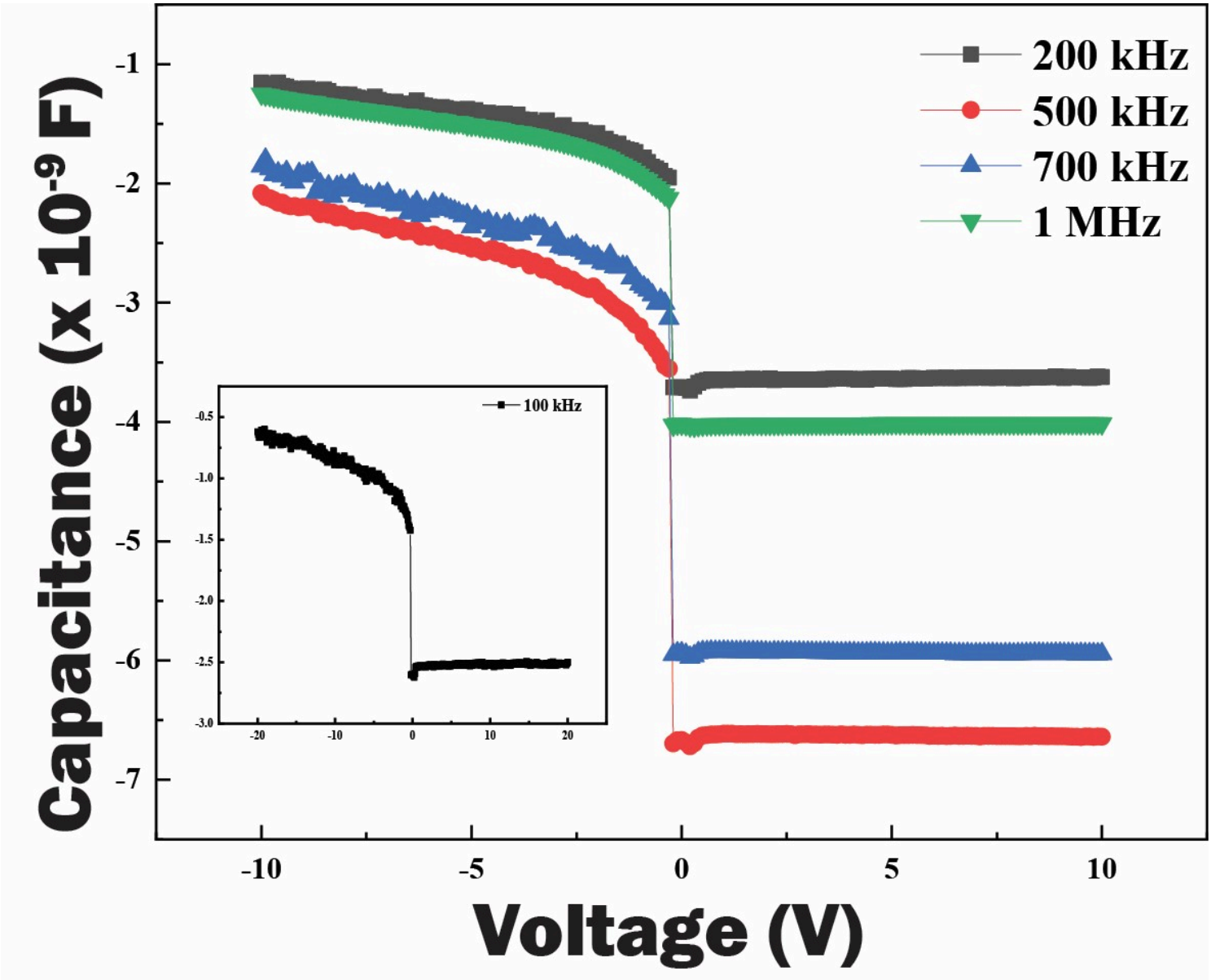


Figure 12

Capacitance–voltage (C–V) characteristics of a barium strontium titanate thin-film interdigital capacitor fabricated on a platinized silicon substrate. A 100 nm thick barium strontium titanate film was first deposited on the platinized silicon substrate by radio-frequency sputtering, followed by the deposition of chromium/gold (40 nm/200 nm) interdigital electrodes through a shadow mask. The C–V characteristics were measured over a bias voltage range of −20 V to +20 V at frequencies of 100 kHz, 200 kHz, 500 kHz, 700 kHz, and 1 MHz. The inset shows the corresponding C–V characteristic measured at 100 kHz.

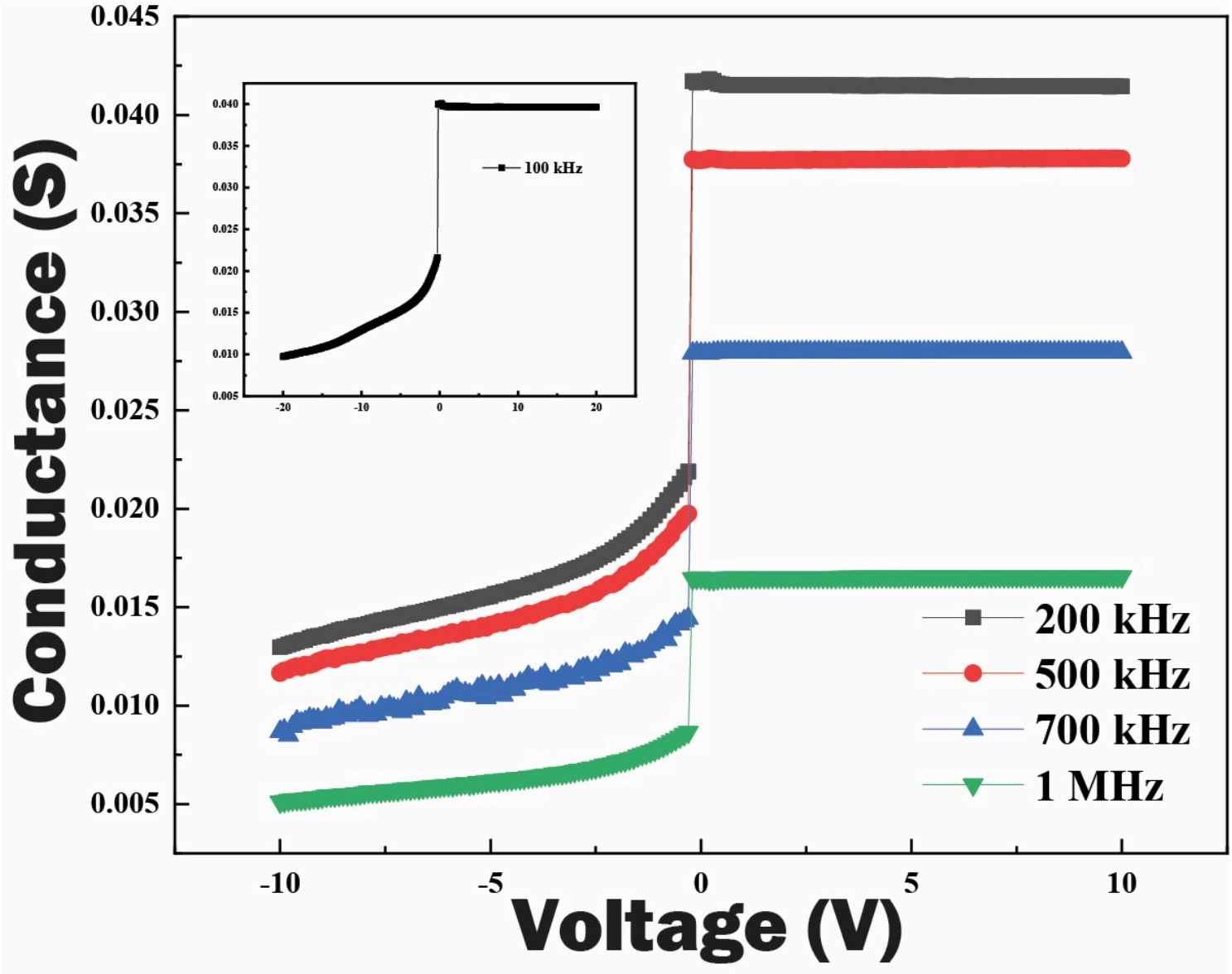


Figure 13

Conductance–voltage (G–V) characteristics of the barium strontium titanate thin-film interdigital capacitor measured over a bias voltage range of −20 V to +20 V at frequencies of 100 kHz, 200 kHz, 500 kHz, 700 kHz, and 1 MHz. The inset shows the corresponding G–V characteristic at 100 kHz.

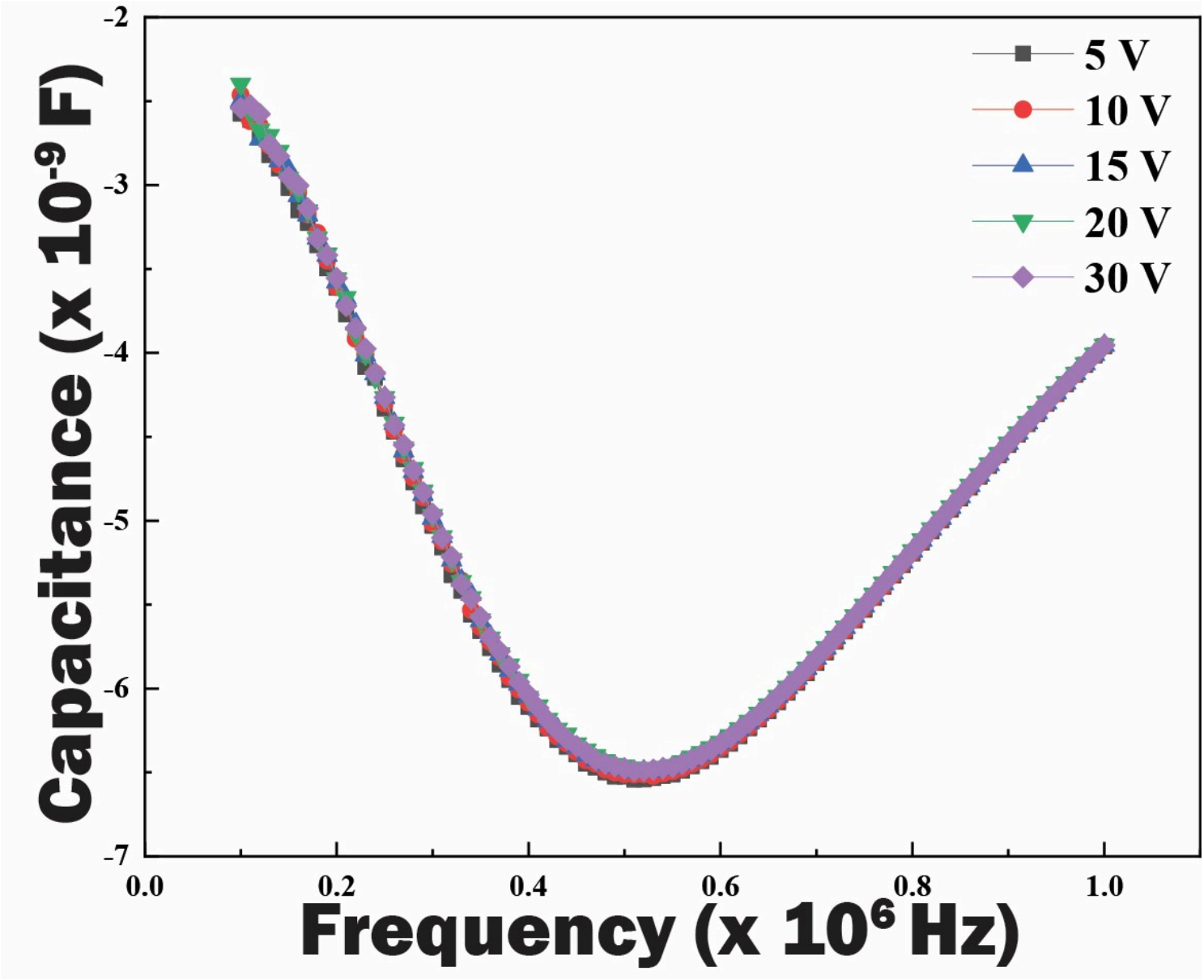


Figure 14

F-requency dependence of the capacitance of the barium strontium titanate thin-film interdigital capacitor measured over the frequency range of 100 kHz to 1 MHz at applied bias voltages of 5 V, 10 V, 15 V, 20 V, and 30 V.

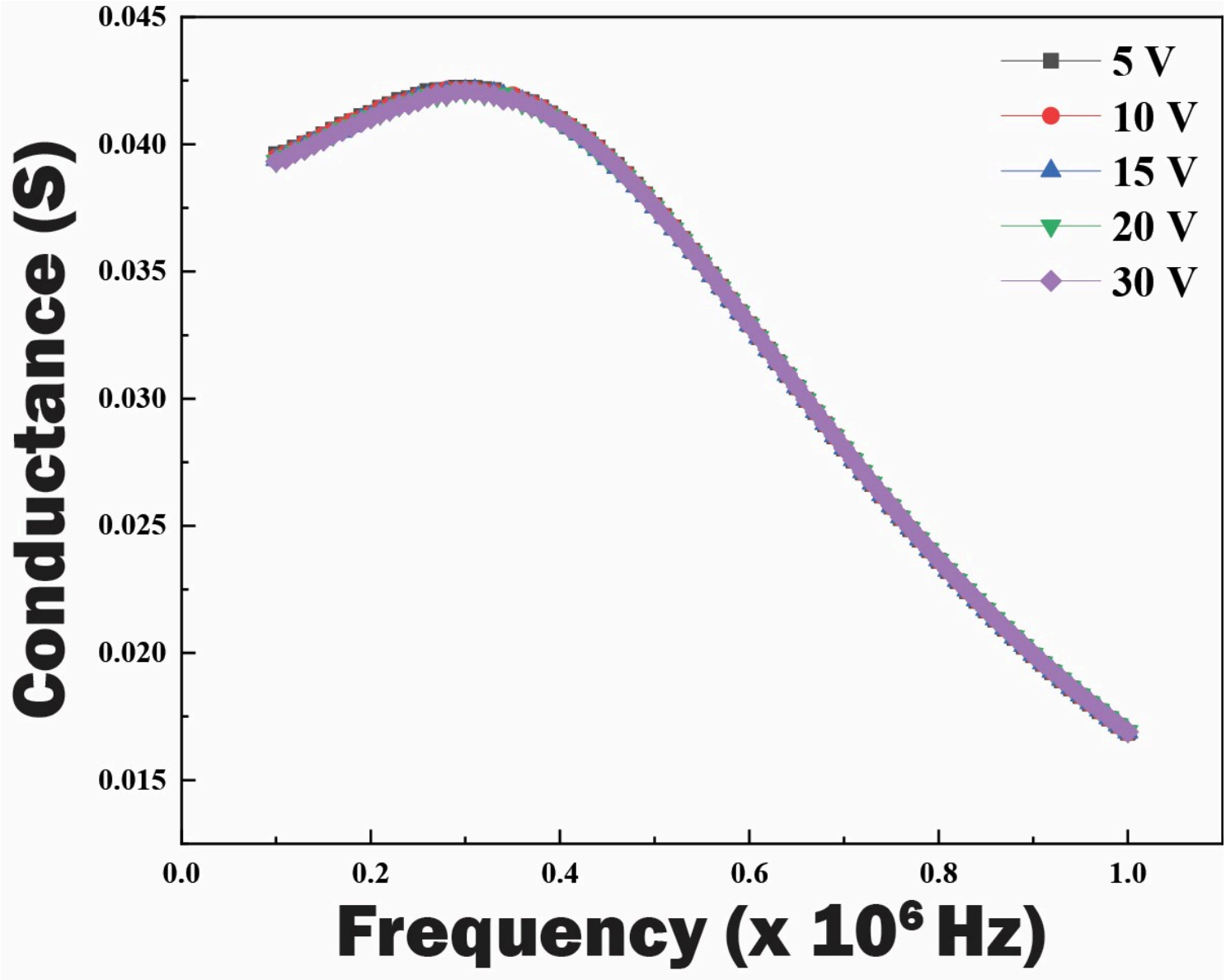


Figure 15

Frequency dependence of the conductance of the barium strontium titanate thin-film interdigital capacitor measured over the frequency range of 100 kHz to 1 MHz at applied bias voltages of 5 V, 10 V, 15 V, 20 V, and 30 V.